

1 *Review*

# 2 **Advances and Perspectives in Chemical Imaging in** 3 **Cellular Environments Using Electrochemical** 4 **Methods**

5 **Robert A. Lazenby**<sup>1</sup> and **Ryan J. White**<sup>1,\*</sup>

6 <sup>1</sup> Department of Chemistry, University of Cincinnati, Cincinnati, Ohio, USA; robert.lazenby@uc.edu

7 \* Correspondence: ryan.white@uc.edu; Tel.: +1-513-556-4837

8 **Abstract:** This review discusses a broad range of recent advances (2013-2017) of chemical imaging  
9 using electrochemical methods, with a particular focus on techniques that have been applied to  
10 study cellular processes, or techniques that show promise for use in this field in the future. Non-  
11 scanning techniques such as microelectrode arrays (MEAs) offer high time-resolution (< 10 ms)  
12 imaging, however at reduced spatial resolution. In contrast, scanning electrochemical probe  
13 microscopies (SEPMs) offer higher spatial resolution (as low as a few nm per pixel) imaging, with  
14 images collected typically over many minutes. Recent significant research efforts to improve the  
15 spatial resolution of SEPMs using nanoscale probes, and to improve the temporal resolution using  
16 fast scanning have resulted in movie (multiple frame) imaging with frame rates as low as a few  
17 seconds per image. Many SEPM techniques lack chemical specificity or have poor selectivity  
18 (defined by the choice of applied potential for redox-active species). This can be improved using  
19 multifunctional probes, ion-selective electrodes and tip-integrated biosensors, although additional  
20 effort may be required to preserve sensor performance after miniaturization of these probes. We  
21 discuss advances to the field of electrochemical imaging, and technological developments which are  
22 anticipated to extend the range of processes that can be studied. This includes imaging cellular  
23 processes with increased sensor selectivity and at much improved spatiotemporal resolution than  
24 has been previously customary.

25 **Keywords:** SEPM; SECM; SICM; biosensors; high-resolution imaging; ion channels; microelectrode  
26 arrays

---

## 28 **1. Introduction**

29 Chemical imaging using electrochemical techniques chiefly comprises scanning electrochemical  
30 probe microscopies (SEPMs). SEPM is made up of a selection of techniques that broadly fall into the  
31 two categories of scanning electrochemical microscopy (SECM) and scanning ion conductance  
32 microscopy (SICM). Numerous modes and sub-techniques, bringing a wealth of accompanying  
33 acronyms, have evolved as a means to add capability to these principle imaging techniques. This  
34 review article addresses the means to bring improved chemical selectivity to electrochemical  
35 imaging, with an emphasis on advances in the field within the last five years (2013-2017). Citations  
36 of earlier significant works are included where relevant.

37 Electrochemical imaging using SEPM employs a scanned probe, with a critical dimension for  
38 imaging on the micro- or nanoscale. This size scale allows the measurement of activity heterogeneity  
39 across a surface, gaining additional insights over bulk electrochemical methods, for which a response  
40 arises from average current over the whole surface. In addition, other surface properties can be  
41 mapped using SEPM and complementary techniques, such as surface morphology, sample  
42 conductivity and atomic force between probe and sample. SECM has been extensively and recently  
43 reviewed [1][2][3], notably for living cells [4] and in neuroscience [5]. Other SEPM reviews include  
44 multifunctional probes for SICM [6], nanoscale electrochemical imaging [7][8][9] and the use of tip  
45 integrated biosensors [10].

46 Noteworthy additions to the SEPM literature in the last five years include the application of  
47 novel and multifunctional electrochemical imaging probes, pushing the limits of spatial resolution  
48 with nanoscale electrochemical imaging, and producing activity movies, where the means of  
49 acquiring an image does not necessarily require the use of a constant applied potential. The last five  
50 years has seen the introduction of several techniques that add chemical selectivity to electrochemical  
51 imaging, particularly in the growing field of biosensors. This review elaborates on the possibility of  
52 combining miniaturized biosensor platforms with high-resolution imaging techniques and methods  
53 of using nanoscale and microscale biosensors amenable to SEPM, even if their full potential is yet to  
54 be realized. This includes signal transduction by ion nanogating sensors, ion channel probes, and  
55 electrochemical aptamer-based sensors.

56 Finally, this review discusses non-scanning techniques employing microelectrode arrays  
57 (MEAs) that typically allow for much higher temporal resolution than SEPM, where whole frames of  
58 an image can be mapped in a few milliseconds (ms). Moreover, each pixel (electrode in an array  
59 device) is measuring simultaneously, as opposed to a mobile scanned probe which can only make  
60 measurements at one position at once. However, due to device fabrication restrictions and the  
61 potential for electrode cross-talk for electrodes with small separation distances, MEAs have much  
62 lower spatial resolution for imaging. This review will cover chemical imaging using electrochemical  
63 imaging methods, offer future perspectives that could be realized with the implementation of  
64 recently developed biosensor probes in SEPM, and discuss imaging using electrode array-type  
65 platforms for spatially resolved chemical measurements in real time.

## 66 2. Scanning Electrochemical Microscopy

67 SECM, pioneered by Bard et al. in 1989 [11], employs a scanned probe with an active electrode  
68 radius of micro- to nanometer dimensions, referred to as an ultramicroelectrode (UME) [12]. The  
69 probe electrode is scanned or positioned over a substrate of interest to build an image of  
70 electroactivity and/or topography. The smaller the active electrode radius, and the closer it is to the  
71 substrate, the higher the attainable spatial resolution for imaging.

72 SECM is a powerful electroanalytical tool to quantitatively study the local electroactivity of a  
73 surface [13], with applications in areas including corrosion science [14], crystal dissolution [15],  
74 biological permeability [16], enzyme activity [17][18], and kinetic rate studies. Redox-active  
75 molecules may be directly detected using an applied potential to oxidize or reduce the molecule at  
76 the probe electrode. Chemical specificity is achieved by the proper selection of a potential to oxidize  
77 or reduce a molecule of interest, which is convenient if few redox species are present. In the  
78 amperometric feedback mode of SECM, a redox-active species is artificially added to the solution,  
79 and the current at the tip electrode provides information on the conductivity and topography of the  
80 underlying substrate. These may be deconvoluted using a tip-substrate distance feedback mechanism  
81 (*vide infra*). There are many modes of SECM, such as the feedback mode [19], generation collection  
82 mode [20], redox competition mode [21] and surface interrogation mode [22]. The advantages and  
83 applications of each method are described elsewhere, and not the focus of the present manuscript.

### 84 2.1. Constant-Distance Imaging Modes

85 Scanning the probe at a fixed height, not accounting for changes in topography of the substrate,  
86 is termed constant-height mode. A significant challenge of SECM is that the measured amperometric  
87 tip current is a convolution of electrochemical activity and tip-substrate separation distance, which  
88 changes due to surface morphology. To overcome this, there has been much effort to introduce  
89 feedback mechanisms that take into account surface morphology and sample tilt to enable constant-  
90 distance imaging, i.e. where the tip-substrate separation distance is kept constant through the scan  
91 by continuous readjustment of the height (z-position). Furthermore, a feedback mechanism that  
92 allows constant-distance imaging also enables the tip to be placed closer to the sample surface  
93 without the possibility of tip-crash.

94 Methods of tip-substrate distance regulation for SECM [23] include simply using the faradaic  
95 current, the use of impedance in alternating current (AC)-SECM [24], the use of oscillating probes in

96 tip-position modulation (TPM)-SECM [25], shear-force SECM [26] and intermittent contact (IC)-  
97 SECM [27] and 3-dimensional super-resolution optical imaging [28]. There are limitations of each of  
98 these techniques, for example the faradaic current is somewhat limited by the fact that the current  
99 response at an electrode is affected by both the tip-substrate separation distance and the  
100 electroactivity of the underlying substrate. AC-SECM uses impedance, thus relies on an  
101 electrochemical signal for feedback. TPM may require additional models that take into account the  
102 nature (i.e. permeability and conductivity) of the underlying substrate [29]. Shear-force SECM  
103 requires specialized probes (flexible glass-coated microelectrodes). IC provides a non-electrochemical  
104 feedback, but relies on physical contact between the tip and substrate, thus occluding soft samples.  
105 There are also combined techniques such as SECM-SICM [30][31] and SECM-atomic force microscopy  
106 (AFM) [32]. However, ion conductance (*vide infra*) and AFM, when coupled to SECM, require  
107 specialized probes that allow for the deconvolution of topography and electroactivity [33]. SECM-  
108 AFM probes are commercially available, although due to the nature of feedback of AFM, imaging  
109 soft cellular samples can be problematic [34].

110 As novel sensor and biosensor platforms become integrated with SECM, which may not use an  
111 amperometric current, a means of sensor positioning becomes more challenging [10]. Shear-force has  
112 been widely adopted as a non-electrochemical and non-contact method to assign tip-substrate  
113 separation [35][36]. In this method of non-contact distance regulation, the tip is oscillated in resonance  
114 laterally using a small amplitude (from below 1 nm up to 5  $\mu\text{m}$ ), and distance-dependent shear-forces  
115 are used to maintain a constant tip-substrate separation. Close to the surface, up to maximum  
116 distances of a few hundred nanometers, hydrodynamic shear-forces impede the free lateral  
117 movement of the tip, and the amplitude of the vibrating tip is used for distance feedback. SECM-  
118 SICM has also gained momentum as a means of achieving distance control for topography (using the  
119 SICM component of the probe) with simultaneous measurement of an electrochemical signal (using  
120 the SECM component of the probe) (*vide infra*).

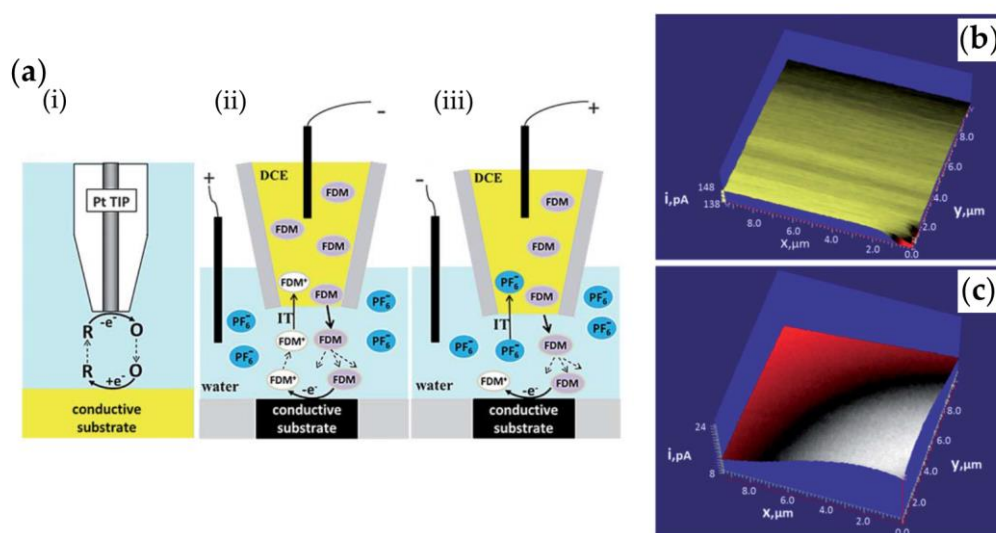
## 121 2.2. Nanoscale Imaging using SECM

122 A long-term trend in SECM technologies has been the production and implementation of smaller  
123 probes, leading to nanoimaging for high resolution (HR)-SECM [37]. The benefits of using  
124 nanoelectrodes are to increase the mass transport to the electrode, due to increased diffusion that  
125 follows a hemispherical field around the electrode, smaller resistance-capacitor (RC) time constants  
126 and low ohmic drops, and to obtain higher spatial resolution images. The radius of a disk electrode  
127 will determine the resolution achievable as well as the distance it is from the substrate, meaning  
128 distance feedback is required for super-high-resolution imaging with nanoelectrodes.

129 When working with probes that have critical electrode dimensions on the nanoscale, special care  
130 should be taken to avoid probe damage caused by electrostatic discharge (ESD) [38]. This has also  
131 been reported for nanopipette-supported pyrolytic carbon tips [39]. Local relative humidity may  
132 explain why such effects are not always reported, since increased humidity will help to reduce ESD  
133 events, which may result in unintended ESD protection. Another consideration for nanoscale  
134 imaging is the effect of temperature changes on the piezoelectric positioners that control tip  
135 movement. An isothermal chamber can be used to suppress the thermal drift of positioners that may  
136 occur over long periods of image acquisition [40]. When such appropriate measures are taken to  
137 ensure a stable tip-substrate nanogap, nanometer scale SECM imaging is feasible [41]. A nanometer-  
138 sized tip, for example, allowed imaging of single 10 or 20 nm gold particles [42]. This size tip also  
139 allows studies of the electrocatalytic activity of individual Pt nanoparticles [43].

140 An interesting development in nanoscale SECM is the use of a nanopipette-supported interface  
141 between two immiscible electrolyte solutions (ITIES). Shigeru and coworkers used a 30 nm diameter  
142 probe (silanized quartz nanopipette) filled with DCE to produce a nanoscale ITIES, and used this to  
143 image a nanoporous  $\text{Si}_3\text{N}_4$  membrane [44]. The ITIES protruded from the tip of a nanopipette, in a  
144 sphere-cap geometry [16], which did not significantly compromise spatial resolution, in part due to  
145 the fact that the tip could be scanned closer to the substrate. Mirkin and coworkers recently  
146 introduced the electron transfer/ion transfer (ET/IT) mode of SECM (Figure 1), which also utilizes

147 ITIES [45]. In their approach, a nanopipette is filled with an organic liquid phase (e.g. 1,2-  
 148 dichloroethane (DCE)) to form an ITIES at the tip opening. A neutral redox species that is sufficiently  
 149 soluble in both the aqueous and organic phases (e.g. ferrocenedimethanol (FDM)) is placed initially  
 150 inside the pipette. Over the course of the experiment, the redox species partitions from the organic  
 151 phase to the aqueous phase, thus can be delivered to the surface during the experiment in close  
 152 proximity to a conducting substrate (within a few tip radii), the redox species FDM can diffuse to and  
 153 oxidize at the surface. The oxidation current measured represents the local ET rate beneath the tip.  
 154 The product of this reaction at the surface, FDM<sup>+</sup>, can diffuse into the pipette by application of an  
 155 applied (negative) potential in the electrode within the pipette, which results in an IT tip current. As  
 156 described, this is referred to as positive IT feedback, since negative IT feedback would refer to a  
 157 reduction reaction at the substrate surface (Figure 1a). The initial absence of (potentially toxic) redox  
 158 mediator in bulk solution, as well as the high spatial resolution make this a suitable mode to study  
 159 biological cells. The ET/IT was shown with proof-of-concept images, including substrate reactivity  
 160 mapping arising from the oxidation of FDM at a Pt substrate (Figure 1).



161 **Figure 1.** ET/IT mode of SECM for imaging a 12.5 μm radius Pt disk substrate. External (aqueous)  
 162 solution contains 1 mM LiPF<sub>6</sub>, and the pipette is filled with 26 mM FDM in DCM (organic). (a)  
 163 Schematics of (i) the feedback mode of SECM (ii) ET/IT mode with positive IT feedback and (iii) ET/IT  
 164 mode with negative IT feedback. (b) Topography image of the substrate, produced by the negative  
 165 IT current of PF<sub>6</sub><sup>-</sup> IT, shows no features. (c) Substrate reactivity map arising from oxidation current of  
 166 FDM partitioning from the filling solution. (Adapted from Ref [45] with permission of The Royal  
 167 Society of Chemistry).  
 168

### 169 3. Scanning Ion Conductance Microscopy

170 Scanning ion conductance microscopy (SICM) was first introduced by Hansma *et al.* in 1989 [46].  
 171 SICM uses the ion current between two quasi-reference counter electrodes (QRCEs) as a feedback  
 172 mechanism for high resolution topographical imaging, where one electrode is placed inside a small  
 173 (10s – 100s nm) pipet and the other is placed in the external bathing electrolyte solution. The method  
 174 is predicated on measuring probe-substrate separation distance dependent changes in ionic current  
 175 to map topographical features of the surface. The lateral resolution of SICM depends on the pipet  
 176 inner opening radius,  $r_i$ , where the fundamental limit of resolution can be approximated to  $3r_i$ , as a  
 177 useful rule-of-thumb for the minimum resolvable object distance [47]. Even so, features smaller than  
 178 the fundamental limit and smaller than  $r_i$ , can be detected, and so values smaller than this limit can  
 179 be found in the literature. The  $3r_i$  limit was obtained using the full width at half maximum (fwhm) of  
 180 the special point spread function (sPSF) of the SICM, which gives a more meaningful value than using  
 181 the separation between the closest edges to two resolved objects [47].

182 SICM, as a contact-free SPM, is particularly attractive for its use in imaging living cells by  
183 avoiding cell deformation, which could occur using atomic force microscopy (AFM) where tip-  
184 sample contact is unavoidable (in standard imaging modes) [34]. Live cells have been imaged by  
185 SICM, and exceptionally high resolution imaging (comparable to scanning electron microscopy) of  
186 the 3D surfaces of tissues have been imaged using hopping mode scans (*vide infra*) [48], although  
187 obtaining chemical information is not trivial. SICM, in the traditional sense, does not provide any  
188 chemical information. More recently, SICM as a standalone technique has been used to image ion  
189 flux that arise from (electro)chemical reactions at an interface [49]. This is a recent advance, that is  
190 not directly chemical imaging, but allows for probing of a reaction of interest at an interface by  
191 monitoring changes in local conductivity at a surface. Information can be inferred about chemical  
192 reactions at a surface, since chemical transformations result in ion fluxes that will influence the ionic  
193 current flowing through the nanopipette imaging probe. In the overwhelming majority of  
194 applications, however, SICM is used purely as a measure of local topography.

195 Generally, in SICM studies, the probe is distance-modulated, so that an alternating component  
196 of the ion current ( $\Delta C$ ) is induced at small tip-substrate separations. Another approach is to modulate  
197 the bias between QRCEs, which eliminates the need to physically perturb the probe position, termed  
198 bias modulation (BM)-SICM [50]. This reduces convection [51], and electro-osmosis and detrimental  
199 effects from extensive polarization of the QRCEs that could occur in distance-modulation SICM.

200 Differential-concentration ( $\Delta C$ )-SICM, in which the electrolyte composition and concentration  
201 inside and outside the nanopipette is not identical, is particularly beneficial for live cell imaging since  
202 the electric field strength can be greatly diminished [52]. This technique also highlights the additional  
203 capability of an SICM probe for the delivery of molecules of interest to a surface (*vide infra*). This  
204 recent expansion of SICM into novel fields beyond topographical measurements has yet to be fully  
205 exploited, although it is a particularly well-suited technique for imaging living systems and single  
206 cells [6].

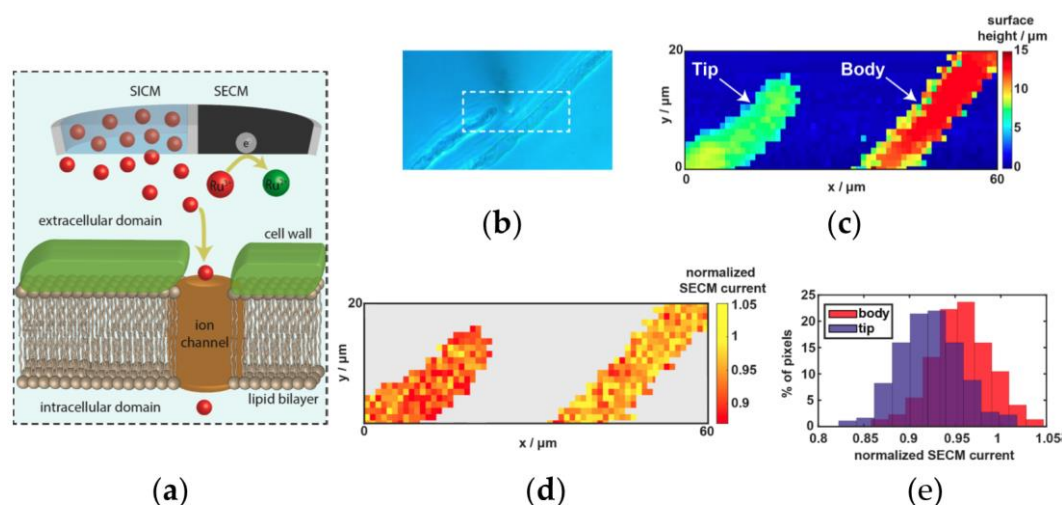
### 207 3.1. Combined SECM-SICM

208 The challenge to image chemical flux using SICM is addressed in different ways. One powerful  
209 way is to bring together the complementary techniques SICM and SECM, by making a probe with  
210 two-components, in combined SECM-SICM. SICM has traditionally been used to image topography,  
211 which also led to its use in combined techniques such as SECM-SICM, whereby chemical information  
212 is gathered using the SECM component of the probe, while the SICM component acts solely to  
213 measure topography. Originally, this was achieved using atomic layer deposition (ALD) of  
214 aluminum oxide to insulate a nanopipette coated with gold (on one side) [30], or similarly with a gold  
215 or Pt nanoring [31]. Focused ion beam (FIB) milling is a robust and reliable method to cut these  
216 nanotips, to give a planar electrode geometry [31][30]. A carbon ring/platinum disk electrode or  
217 carbon ring/nanopore electrode can be fabricated in which the electrode surfaces are also exposed  
218 using FIB milling [53]. FIB milling of carbon nanoelectrodes, prepared by chemical vapor deposition  
219 (CVD), has enabled high-resolution SECM imaging [39]. Pt nanotips may also be shaped using FIB,  
220 to achieve a lower insulating sheath radius for use with SECM [54].

221 More recently, the dual-barrel pipet with pyrolyzed carbon in one of the two barrels (for the  
222 SECM component) has garnered interest due to the ease and speed of probe fabrication [55]. These  
223 double barrel carbon nanopipettes (DBCNPs), made using a quartz theta-pipette, can be used for  
224 localized chemical delivery, by filling the barrel used for SICM feedback with a molecule of interest.  
225 Nanopipette delivery in this form is affected by surface charge [56].

226 When SICM is coupled to SECM for investigation of cellular uptake, SICM can also be used to  
227 deliver species, loaded in the pipet barrel [57]. For example, Unwin and coworkers used an SECM-  
228 SICM probe to deliver hexaammineruthenium(III) ( $[\text{Ru}(\text{NH}_3)_6]^{3+}$ ) to a *Zea mays* root hair cell (Figure  
229 2). The  $[\text{Ru}(\text{NH}_3)_6]^{3+}$  migrates out of the SICM barrel of the pipet, controlled by the applied potential  
230 to the electrode inside this barrel, and can be reduced at the SECM carbon electrode. Over an inert  
231 surface, the reduction current is higher than in bulk solution, due to the reduced diffusion field,

232 whereas over a cell, there is a loss of  $[\text{Ru}(\text{NH}_3)_6]^{3+}$  into the cell via membrane transport (e.g. through  
 233 ion channels), which results in an SECM current that is lower than in bulk solution.



234

235 **Figure 2.** A dual-barrel SECM-SICM probe is used to visualize molecular  $[\text{Ru}(\text{NH}_3)_6]^{3+}$  delivery and  
 236 uptake at two regions of a single *Zea mays* root hair cell. (a) Schematic of the SECM-SICM setup,  
 237 showing the probe positioned over a cell, in which  $[\text{Ru}(\text{NH}_3)_6]^{3+}$  can diffuse/migrate from the  
 238 delivering SICM barrel to the cell wall. Simultaneous measurement of  $[\text{Ru}(\text{NH}_3)_6]^{3+}$  reduction at the  
 239 SECM electrode surface is made during the approach to the surface. This is compared to bulk (steady-  
 240 state) current measurement for quantification. (b) Optical microscope image of the root hair cell. The  
 241 dashed line marks the scanned area. (c) Topography image using the z-position at the end of each  
 242 normal approach curve. (d) SECM current image over the sample, normalized to a bulk measurement  
 243 at each pixel (current at the start of each normal approach curve). (e) Histogram plots of the  
 244 normalized SECM current at each of the two regions of the root hair cell, labelled as “tip” and “body”  
 245 in part (c). (Adapted with permission from Ref [57]. Copyright (2017) American Chemical Society).

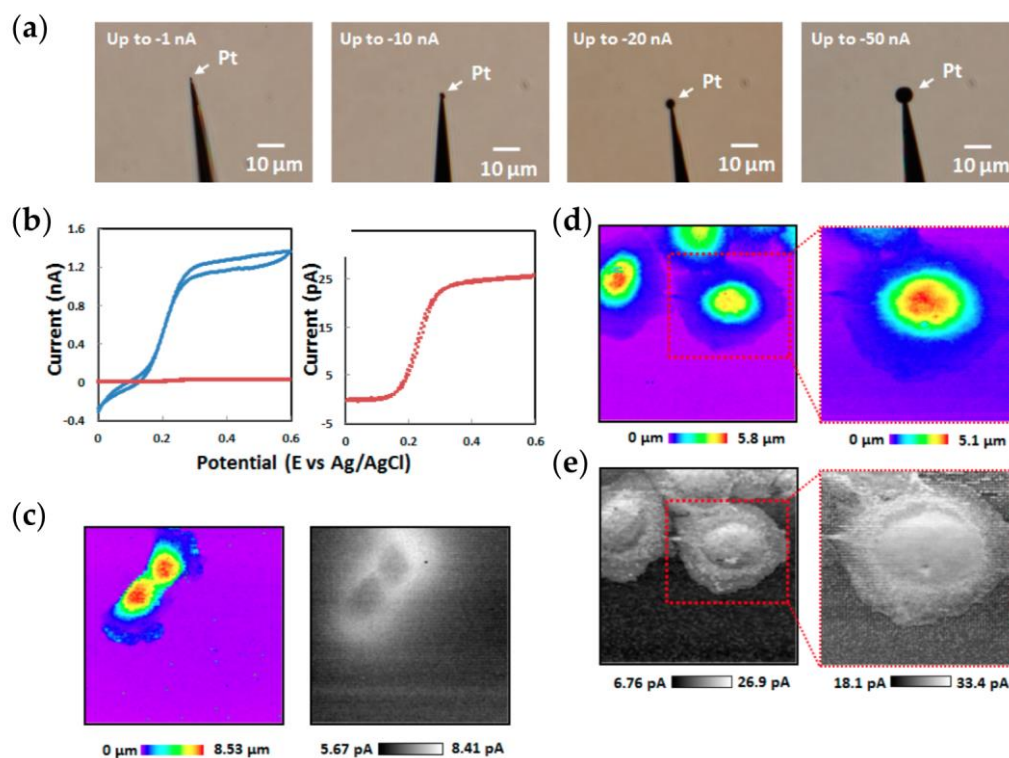
### 246 3.2. High-resolution SECM-SICM

247 The success of high-resolution electrochemical imaging using SEPM, with quantitative current  
 248 measurements, depends on the design and geometry of the probe used. As the variety of probes used  
 249 in SEPM platforms has increased, understanding the exact geometry has become increasingly  
 250 important for quantitation of the current response [58]. Recently, comprehensive tip characterization  
 251 of SICM probes has been explored using transmission electron microscopy (TEM) and ion  
 252 conductance measurements, taking into account the effects of surface chemistry on the tip current  
 253 response [44][58][59].

254 Another approach to improving tip geometry is the deposition of Pt on single barrel carbon  
 255 probes, which can be useful for the analytical detection of hydrogen peroxide [60]. Platinized carbon  
 256 nanoelectrode probes possess very thin insulating sheaths, which are required for high-resolution  
 257 SECM imaging [61], and deposition on recessed carbon electrodes offers additional control on the  
 258 final tip geometry (recession depth) [9]. Pt-deposited carbon nanoelectrode SECM-SICM probes have  
 259 been used to image hydrogen peroxide, exploiting the oxygen reduction reaction (ORR) on Pt [62].

260 Matsue and coworkers fabricated sphere-shaped Pt electrodes of different sizes, using highly  
 261 controllable electrochemical deposition of Pt on the carbon-filled barrel of dual barrel SECM-SICM  
 262 probes. Probes of increased sphere diameter are produced at increased current. This sphere-capped  
 263 probe geometry led to electrodes with much improved sensitivity as compared to the bare carbon  
 264 nanoelectrodes, due to enhanced faradaic current (Figure 3) [63]. It is also worth mentioning that  
 265 these probes with protruding geometries maintain high resolution for imaging, yet have much  
 266 improved sensitivity than a planar disk geometry, which should prove invaluable for using  
 267 miniaturized biosensors for chemical imaging.

268



269  
 270 **Figure 3.** Dual barrel SECM-SICM probes are used to image immunocytochemically-stained  
 271 EGFR proteins on A431 cells. (a) SECM-SICM probes with Pt sphere electrodeposited on the carbon  
 272 SECM nanoelectrode, with increasing (left-right) amount of Pt deposition. (b) Cyclic voltammogram  
 273 of a bare carbon nanoelectrode (red) and a Pt-deposited probe (blue) at -10 nA final deposition. (c)  
 274 Topographic (left) and electrochemical (right) image of A431 cells acquired using a bare carbon  
 275 electrode over an  $80 \times 80 \mu\text{m}$  scan area. (d) Topography and (e) electrochemical images of a A431 cells  
 276 acquired using a Pt-deposited electrode, where the scan area is  $75 \times 75 \mu\text{m}$  on the left and  $50 \times 50 \mu\text{m}$   
 277 on the zoom-in (right). (Adapted with permission from Ref [63]. Copyright (2015) American Chemical  
 278 Society).

#### 279 4. Functional and Chemical Specific Probes for SECM

280 The development of electrochemical biosensors to quantitatively detect new targets has been a  
 281 growing field that seeks to attain improvements in the fundamental analytical figures of merit, which  
 282 include sensitivity, selectivity, limit of detection (LOD) and signal-to-noise ratio (SNR). As sensors  
 283 become smaller, they may be implemented into an SEPM for chemical imaging, provided that the  
 284 figures of merit are sufficient for an observable and meaningful measurement [64]. Pushing the  
 285 spatial resolution of an imaging sensor can have a detrimental effect on other figures of analytical  
 286 merit; in particular for the sensitivity of sensors predicated on surface-modified electrodes without  
 287 the use of signal amplification.

288 Electrochemistry is a powerful tool in understanding neurotransmission, due to the spatial and  
 289 temporal superiority over other techniques [65]. Carbon fiber electrodes are widely used to monitor  
 290 neurotransmitters, catecholamines and their metabolites, with a huge body of work focused on  
 291 dopamine. Selectivity in the measurement arises from the unique redox potentials of the redox-active  
 292 molecules of interest. This amperometric measurement may lack the selectivity to discriminate  
 293 specific molecules with closely separated redox potentials, although fast scan cyclic voltammetry  
 294 (FSCV) does allow better selectivity within a measurement. Interference from certain species can be  
 295 minimized using chemical additives to the media, such as ascorbate oxidase to avoid the interference  
 296 of ascorbic acid (present in extracellular media) [66]. However, methods of achieving better selectivity  
 297 as well as addressing the need to detect non-electroactive species requires modified probes such as  
 298 electrochemical biosensors.

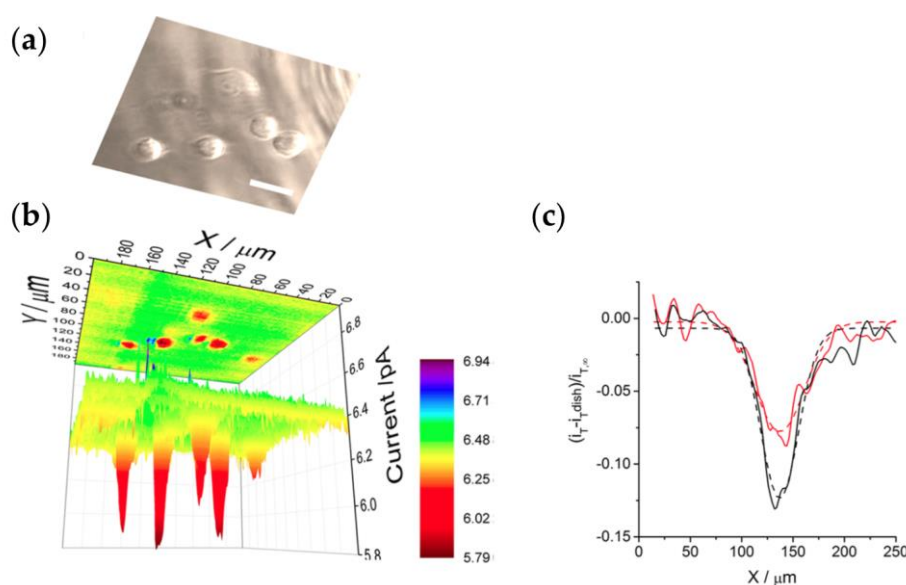
299 An example of using a functional probe for imaging is the use of a dual electrochemical  
300 microsensor to simultaneously image oxygen and pH over the surface of a rat kidney [67]. The probe  
301 consisted of two recessed 10  $\mu\text{m}$  diameter Pt electrodes, separated by 50 – 70  $\mu\text{m}$ . One was modified  
302 with electrodeposited Pt followed by a coating of hydrophobic photocured polymer. This portion of  
303 the probe was used for amperometric detection of  $\text{O}_2$ , while the second was modified with an  
304 electrodeposited layer of iridium oxide ( $\text{IrO}_2$ ) for pH mapping. The highly porous surface  
305 modification (Pt or  $\text{IrO}_2$  layers) improved sensitivity and provided almost immediate response times  
306 of  $t_{90\%} = 0.17 \pm 0.005\text{s}$  for the  $\text{O}_2$  sensor and  $t_{90\%} = 0.43 \pm 0.09\text{s}$  for the pH sensor. A similar approach  
307 has been used for dual barrel SECM-SICM probes that can function as a pH sensor, exploiting the pH  
308 sensitivity of  $\text{IrO}_2$  [68].

#### 309 4.1. Enzyme Modified Probes for Chemical Imaging in Scanning Electrochemical Microscopy

310 The enzyme activity of an enzyme-modified surface can be mapped using SECM [69], but  
311 electrode scanned probes modified with enzymes can themselves provide a means of achieving  
312 specific analyte recognition. Enzymes can be attached to the electrode surface directly, by covalent  
313 bonding, or by entrapment of the enzyme in a polymer film over the electrode surface. Immobilized  
314 enzyme sensors for species-selective have been implemented in the SECM [70], for example an  
315 enzymatic amperometric biosensor was used to measure the release of endogenous D-serine in the  
316 brain of stage 48 albino *Xenopus laevis* tadpoles [71]. This electrode had an appropriate dimension (25  
317  $\mu\text{m}$  diameter), and gave good temporal resolution, to be used as a probe in SECM [72]. The probe  
318 itself consisted of a 25  $\mu\text{m}$  diameter Pt disk electrode with an electrodeposited layer of poly-*m*-  
319 phenylenediamine (PPD) and an adsorbed enzyme layer of D-amino acid oxidase from *R. gracilis*  
320 (RgDAAO). Enzyme immobilization onto Pt UMEs by electropolymerization or casting was also  
321 performed to image single live cells using SECM [73].

322 The incorporation of biosensors on the micro- and nanoscales will find more use in SECM  
323 techniques, provided that achieving reproducible sensors with reasonable response times at the  
324 sizescale required for imaging is feasible. There are some examples of types of biosensors that could  
325 be used for chemical imaging that work using enzyme-modification [74]. An enzyme coating was  
326 deposited onto a 10  $\mu\text{m}$  Pt UME, either by cross-linking, electropolymerization or adsorption, and  
327 was used for imaging glucose and lactate (Figure 4) [75]. However, there remain challenges and  
328 opportunities in the miniaturization of enzyme-based sensors [76].

329  
330  
331  
332



333

334 **Figure 4.** Imaging of glucose uptake by live cells using an enzyme-modified probe in SECM. (a)  
335 Optical microscope image of the scanned area covering several MCF10A cells. Scale bar is 30  $\mu\text{m}$ ; (b)  
336 Constant height SECM image of glucose uptake of the MCF10A cells, using electropolymerized 10  
337  $\mu\text{m}$  Pt GOx-UME biosensor; (c) Single line scans of the normalized (to steady-state bulk) current of  
338 the biosensor probe over a single cell. Black lines represent the convoluted activity and the  
339 topography contributions of the current and red lines represent only the topographical contribution.  
340 (Adapted with permission from Ref [75]. Copyright (2017) American Chemical Society).

#### 341 4.2. Potential for Biosensor Probes in Scanning Electrochemical Microscopy

342 There are currently very few examples of scanning micro- or nanoscale biosensors for imaging  
343 applications. The key challenges are the miniaturization of the sensor, and implementing tip-  
344 positioning feedback. Noteworthy examples include carbon microelectrodes that have been modified  
345 with [NiFe]-hydrogenase embedded in a viologen-modified redox polymer hydrogel to produce a  
346 microbiosensor for hydrogen detection with high sensitivity (30 times higher current associated with  
347 hydrogen generation as compared with a bare Pt microelectrode) in scanning photoelectrochemical  
348 microscopy (SPECM) [77]. Also, a UME functioned as an insulin sensor, made by incorporating a  
349 multiwalled carbon nanotube (MWCNT) and dihydropyran film. This sensor achieved real-time  
350 direct electrochemical detection of insulin concentration within extracellular media [78].

351 For the development of novel sensors with high specificity to a target molecule, aptamers are a  
352 promising candidate for incorporation into electrochemical imaging probes. Aptamers are short  
353 single-stranded DNA or RNA oligonucleotides or peptides that are able to bind to specific molecules.  
354 They can be engineered to undergo reversible conformational changes when binding to a specific  
355 target molecule, which makes them a promising class of biosensor for highly selective chemical  
356 imaging. Electrode surfaces modified with nucleic acids, at a sizescale that would allow for operation  
357 with SECM, have been produced. For example, Kelley and coworkers produced nanostructured  
358 microelectrodes with diameters between 10 and 100  $\mu\text{m}$ , which could be made into specific sensors  
359 for different bacterial targets by immobilization of a particular peptide nucleic acid (PNA) on the  
360 surface [79]. Electrochemical aptamer-based (E-AB) sensors, which typically operate on the  
361 macroscale, can also be achieved on micron sized electrodes [80]. Electrochemical DNA (E-DNA)  
362 sensors have been produced on recessed Pt substrates as low as 10 nm, but with gold  
363 electrodeposition used to greatly increase the surface area (to 1000  $\mu\text{m}^2$  as measured by gold oxide  
364 reduction in CV) [81]. As smaller biosensors become more widely used, applications in chemical  
365 imaging are expected to increase.

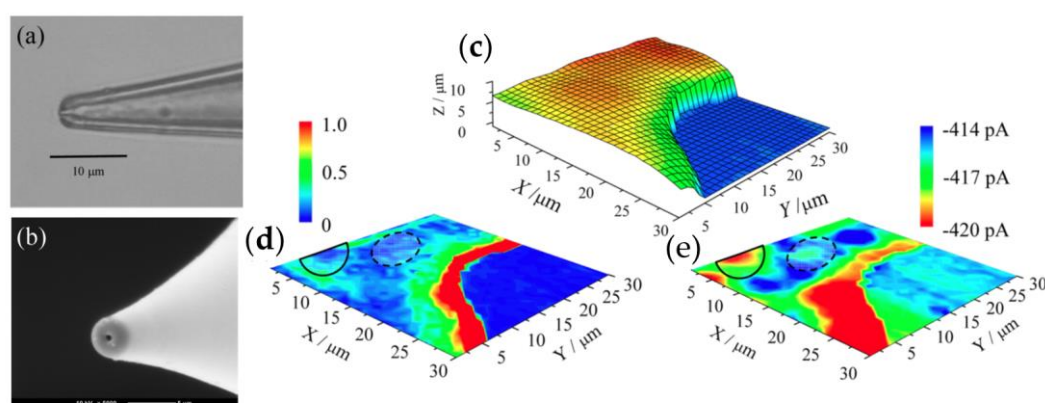
366 E-AB nanosensors have been fabricated on single Au nanowire electrodes; a small sized  
367 footprint electrode that takes advantage of the protruding geometry for improved sensor sensitivity  
368 [82]. In this example however, while the sizescale of the E-AB nanosensor is amenable to high  
369 resolution imaging, the signaling mechanism for the ATP-selective E-AB sensor would not be  
370 appropriate for imaging. The E-AB nanosensor was made using a duplex DNA, which could  
371 dissociate in the presence of ATP, meaning methylene blue (MB)-labeled aptamer would need to be  
372 re-added (in the absence of ATP) for regeneration of the signal.

#### 373 4.3. Scanning Ion-Selective Electrode Technique (SIET)

374 Small-scale ion-selective electrodes (ISEs) provide another means of achieving specific detection  
375 and imaging when coupled with SEPM. The ISEs may be glass membrane, solid state, liquid-based  
376 or compound electrodes. Ion-selective microelectrodes (ISMEs) operate on the sizescale that makes  
377 them useful for SECM and imaging. Bard and coworkers introduced scanning ISMEs (1  $\mu\text{m}$  tip  
378 diameter) in 1995, selective for ions such as  $\text{NH}_4^+$ ,  $\text{K}^+$  and  $\text{Zn}^{2+}$ , and coupled with SICM for feedback  
379 [83].  $\text{Mg}^{2+}$  ISMEs have been demonstrated for potentiometric SECM monitoring of Galvanic corrosion  
380 processes [84]. Carbon-based solid-state  $\text{Ca}^{2+}$  ISEs [85], and dual-electrode pH sensors with fast  
381 response times were used to quantitatively map the chemical environment at a model substrate  
382 bioactive glass (BAG) [85].

383 ISMEs are potentiometric probes with high impedance, which, in addition to the capacitance of  
384 the measuring system, will result in long response times (several seconds). As a result, the imaging  
385 speeds attainable without image distortion will be limited [86]. Long scanning times are often a  
386 requirement for imaging using potentiometric SECM, which often means dynamically changing  
387 systems cannot be studied. Thus, there is great effort to reduce the response time of the ISME probe,  
388 as well as signal processing methods to deconvolute a raw distorted image obtained at high scan rate  
389 [87]. This type of correction, in which images can be obtained using systems that have not reached  
390 equilibrium at each pixel, can be obtained, at an order of magnitude faster than without the  
391 deconvolution. Temporal resolution is an important consideration for imaging, and especially so with  
392 potentiometric probes such as ISEs. Ions and anions must be measured slowly (0.5 to 1 seconds per  
393 pixel) due mainly to mechanical disturbance of the ion concentration gradient when the probe is  
394 moved but also to the time constant of the electrode, which is tenths of seconds for liquid ion  
395 exchanger (LIX) electrodes.

396 For improved spatial resolution, nano-ISEs have been prepared for imaging  $K^+$  flux in living  
397 human embryonic kidney 293 cells (HEK293) (Figure 5) [88]. In this study, a 200-300 nm inner radius  
398 capillary was used, and each pixel in the image was the average of a 0.4 s interval measurement  
399



400

401 **Figure 5.**  $K^+$ -selective nanoelectrodes were used to simultaneously image topography and  $K^+$  flux  
402 using SECM. (a) Optical microscopy image of a glass capillary used as an ion-selective nanoelectrode  
403 for SECM. (b) SEM micrograph of the same tip. (c) Topography image. (d) Maximum gradient of the  
404 sample surface image. (e) SECM current image of HEK293 cells. (Adapted with permission from Ref  
405 [88]. Copyright (2014) American Chemical Society).

406

## 407 5. Biosensor Probes in Scanning Ion Conductance Microscopy

### 408 5.1. Functionalized Glass Nanopipettes for Ion Gating Based Sensors

409 Nanopipettes can be functionalized, typically with a protein that binds to a specific target and  
410 undergo a signal change to function as a sensor, which has been termed signal transduction by ion  
411 nanogating (STING). There are a few examples of nanopipettes modified with proteins to produce  
412 reversible sensors that respond to a specific target molecule. For example, glucose oxidase has been  
413 surface immobilized on the inner walls of a glass nanopipette to function as a glucose sensor, used  
414 for intracellular detection of elevated glucose levels in single cancer cells [89]. Also, a glass  
415 nanopipette was functionalized with calmodulin protein which reversibly binds to cations such as  
416  $Ca^{2+}$ , resulting in a decrease in current at a negatively biased pore [90]. While a large area of the glass  
417 nanopipette is functionalized with an antibody, DNA, peptide or aptamer, due to a high impedance  
418 of nanopipettes, the sensitivity of the device is confined to within a micron of the 50 nm tip orifice.  
419 These probes offer the sizescale and fast response times required for SEPM imaging, but functional  
420 mapping at the nanoscale has yet to be realized in this emerging field. Nanopipettes functionalized

421 with specific recognition elements are a promising developing area of research that could yield  
422 biosensors capable of imaging at the single cell level [91]. In particular, aptamer-functionalized  
423 nanopipettes demonstrate reversible response to a target, not readily observed with antibody-  
424 modified nanopipettes [92]. Pourmand and coworkers used the ion current through an aptamer  
425 functionalized STING sensor nanopipette to demonstrate reversible and quantitative detection of  
426 thrombin [93]. This technology has been limited to bulk solution measurements thus far, but imaging  
427 using the principles of STING should be practically achievable, since these sensors can be readily and  
428 cheaply made at nanometer dimensions (typically 100 nm diameter at the tip orifice) and they  
429 demonstrate reversibility to changing target concentration, with a response time of a few seconds  
430 (faster response times may be expected with smaller target molecules).

### 431 5.2. Ion Channel Probe-Based Scanning Ion Conductance Microscopy

432 A particularly exciting and emerging recent development in the field of SICM is the use of a  
433 probe that supports a lipid bilayer at the tip, into which ion channels are embedded, thus providing  
434 specificity and very high signal to noise ratios. Ion channels are nature's nanopores that can be  
435 exploited as nanoscale biosensors by monitoring changes in an ion current that flows through the  
436 channel(s) [94]. Different membrane proteins that bind to specific targets, including previously  
437 unattainable molecules, can be incorporated into a lipid bilayer to enable molecule-specific nanoscale  
438 biosensors with single molecule sensitivity.

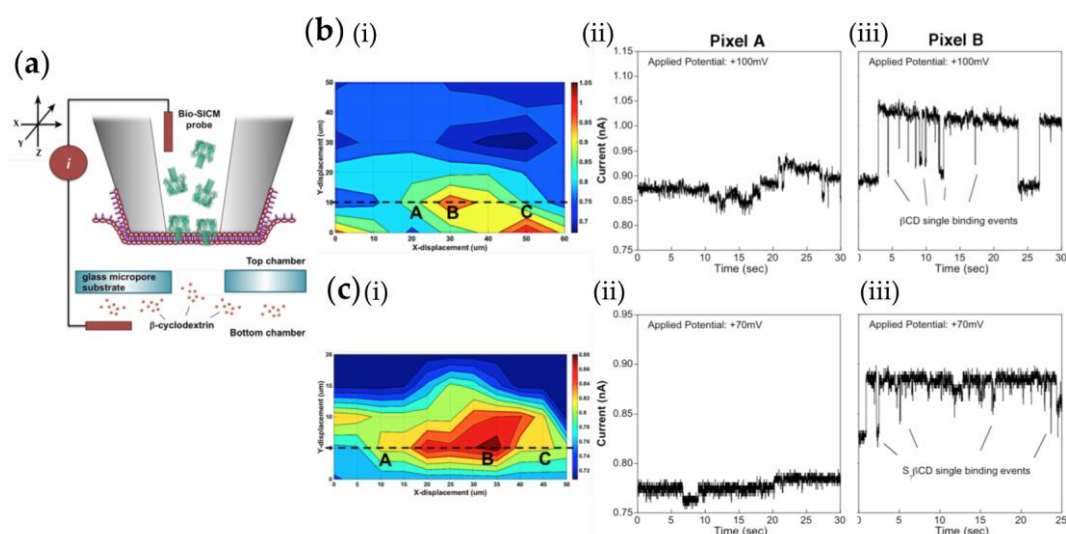
439 A lipid bilayer can be formed at the end of a glass micropipette [95,96], which can then be  
440 employed in a scanning probe microscope, such as a scanning ion conductance microscope (SICM)  
441 [46]. Combining an ion channel probe with SICM allows for localized quantitative concentration  
442 mapping of a target analyte. Recently, ion channel-based probes (ICPs) for SICM have been  
443 introduced, which can operate either using a single-barrel [97,98] or a dual-barrel pipette [99]. The  
444 dual-barrel approach offers the potential advantages of decoupling the SICM feedback current and  
445 ICP current measurements, and allowing operation with fewer ion channels which may sometimes  
446 be beneficial. These approaches allow topography imaging [97], as well as simultaneous topography  
447 and selective molecular flux mapping [98,99]. These ICPs for SICM provide a means to quantitatively  
448 elucidate mechanistic and spatial information on important biological transport processes.

449 An alpha-hemolysin ( $\alpha$ HL) ion channel was incorporated into a lipid bilayer at the opening of a  
450 glass micropore pipette, and was used to image  $\beta$ -cyclodextrin ( $\beta$ CD) and heptakis(6-O-sulfo)- $\beta$ -  
451 cyclodextrin ( $S_7\beta$ CD) diffusing out of a glass micropore substrate (Figure 6) [98]. These cyclodextrin  
452 molecules can enter and exit the  $\beta$ -barrel region of the  $\alpha$ HL protein, causing a transient blocking of  
453 ion current through the pore. As a proof-of-concept, the imaging spatial resolution was fairly poor,  
454 although this was partially due to the requirement to spend a sufficient amount of time at each pixel  
455 (30 seconds) in order to collect enough events for some qualitative (if not quantitative [100]) analysis  
456 of ligand concentration by capturing channel-blocking events in the current-time signal. The  $\alpha$ HL ion  
457 channel is very widely studied [101], but does not have the ability to bind to specific molecules of  
458 interest, thus lacks practical application as a biosensor.

459 Baker and coworkers used human embryonic kidney293 cells transfected with BK channels  
460 (large-conductance, voltage, and calcium-activated potassium channels) onto which patch clamp  
461 measurements could be made. Using suction, membrane patches could be extracted from single cells,  
462 and probes were made in both the outside-out and inside-out configurations [99]. Using a double-  
463 barrel probe for membrane-patching required the pipettes to be fire-polished to minimize  
464 capacitive artifacts and facilitate a gigaseal membrane across the opening [99]. This method of  
465 membrane patching opens up the range of ion channels that can be incorporated into a ICP [99][102].  
466 The library of proteins that has been exploited for use in nanopore-based biosensors is still small.  
467 More challenging proteins, such as heat shock cognate 70 (Hsc70) which forms a multi-conductance  
468 state pore in the presence of adenosine triphosphate (ATP), can also be incorporated into a lipid  
469 bilayer. For this non-well behaved channel, the charge flux has been monitored as a means to quantify  
470 ATP concentration from the current-time response [103].

471

472



473

474

**Figure 6.** Single barrel ion channel probes can be used to image a substrate. (a) Schematic of the single-barrel ICP SICM set up, showing a probe above a glass micropore containing 100 mM of  $\beta$ CD. (b) (i) Average current image shows the effect of changing topography, with highest current directly over the pore. (ii) Current-time traces of the ICP barrel obtained at (i) pixel A, over the glass substrate and (ii) pixel B, directly over the micropore where the observed binding event frequency is highest. (c) As for (b), except  $S_7\beta$ CD was used in the pore instead. (Adapted with permission from Ref [98]. Copyright (2016) American Chemical Society).

481

482

There are significant challenges that make chemical imaging using ion channel nanopores difficult to implement. It is highly conceivable that the use of specific ligand-gated ion channels will find further use with complementary techniques such as SICM for imaging, where the SICM component of the probe functions for topography mapping of a substrate, and the ion channel component of the probe functions to give quantitative chemical information at particular locations of a sample. Various attempts at quantifying ion channel activity to specific species concentration, including for multiple channels [100], have been demonstrated [102][103]. Dual-barrel ICPs are thus required to decouple the distance feedback from the ion channel activation so that quantitative chemical imaging can be realized.

491

492

493

## 494 6. Advanced Scanning Modes of SEPM Including Fast Scanning and Imaging Movies

### 495 6.1. Hopping Imaging Modes of SICM and SECM

496 A hopping mode of scanning was conceived as a means to probe topographically challenging  
 497 substrates [104], since the probe performs a short approach curve at every pixel in the image. This  
 498 minimizes the time the probe spends close to the substrate, but is also advantageous in that current  
 499 information can be collected during the approach and plotted to give chemical concentration  
 500 information away from as well as at the surface, as in hopping intermittent contact (HIC)-SECM [105].  
 501 This was first demonstrated using 4-dimensional shear-force-based constant-distance (4D SF/CD)-  
 502 SECM, in which shear-forces were used to obtain sample topography and images were collected at a  
 503 series of (constant) distances from the surface [106]. The same approach has been termed depth scan  
 504 mode for imaging topography of cells [107] and tracking live cell response to  $Cd^{2+}$  concentrations  
 505 [108][109].

506 Collecting a measurement at the surface, and a second measurement in bulk solution (i.e. far  
507 enough away from the surface that any surface feedback effects have little to no effect on the  
508 measurement), allows self-referencing of the probe. At each pixel in the image, the probe is calibrated,  
509 so that changes in probe response over time can be accounted for, which is especially important for  
510 lengthy experiments or measurements performed in living systems that may be more dynamic and  
511 change over time [57].

## 512 6.2. Fast Scanning and Imaging Movies Obtained with SEPM

513 Mauzeroll and coworkers, used probe speeds in SECM of  $50 \mu\text{m s}^{-1}$  to scan linescans of a single  
514 HeLa cell [110]. For SECM, the challenge of high-speed imaging remains the availability of models  
515 that take into account the effects of increased and forced convection, fluid flow and changes to  
516 diffusion, caused by the probe moving at increased velocities [111][110][112].

517 Typical hopping scans withdraw the tip after every approach to the surface by a constant height,  
518 which negatively affects temporal resolution. Matsue and coworkers used a new scanning algorithm  
519 to perform hopping SICM at high speeds, through which the amplitude of the tip withdrawal was  
520 controlled [113]. Briefly, very short approaches were used, which could result in a contact between  
521 tip and sample. If this happens, the tip could be withdrawn a few steps (in the x-direction) and  
522 approaches with a greater withdrawal amplitude can be used for that region of more challenging  
523 topography on the surface. Since smoother regions can be scanned faster, a topography image was  
524 collected every 18 s ( $64 \times 64$  pixels at  $10 \times 10 \mu\text{m}$  for an image of microvilli on an A431 cell). There are  
525 other examples of creative scanning modes such as using algorithms to correct for image skew that  
526 could be a problem with potentiometric SEPM at fast scan rates, provided the object being imaged is  
527 symmetrical [114], and using the predicted movement of a pipette during imaging over parts of a  
528 sample that the topography does not change much [115].

529 Another recent theme in electrochemical imaging has been producing quantitative movies of  
530 activity of a sample. Each frame in a movie can correspond to a potential in a voltammogram,  
531 obtained by performing linear sweep voltammetry (LSV) or cyclic voltammetry (CV) at every pixel  
532 in the scan (position on the substrate). The frames can be made from repetitive scans over an area of  
533 interest, where each frame of the movie is a new scan of the surface, which may change over time.  
534 Alternatively, the frames can be made by performing dynamic voltammetric measurements at each  
535 pixel in a single scan, such as linear sweep voltammetry (LSV) or cyclic voltammetry (CV), to  
536 construct a movie in which each frame corresponds to a different potential.

537 Originally conceived as a dual-barrel pipette based technique [116], and most recently in a single  
538 barrel format [117], scanning electrochemical cell microscopy (SECCM) is a droplet cell-based  
539 imaging technique. The advantages of a droplet electrochemical cell are that the contact area of the  
540 meniscus defines the area of the substrate that is probed at each pixel. This is in contrast to techniques  
541 like SECM and SICM, in which the entire surface needs bathing in solution. This does limit the  
542 technique to non-biological samples, since cells require a stable solution-based environment for  
543 healthy and proper function. Movies of electrochemical activity have been performed using LSV-  
544 SECCM for the hydrogen evolution reaction (HER) on  $\text{MoS}_2$ , to study the intrinsic activity of the edge  
545 and basal plane sites [117][118]. Unwin and coworkers have implemented a non-raster-scan pattern  
546 following a spiral trajectory for faster imaging with SECCM [119]. Image sequences were collected  
547 with a frame rate of 0.24 fps, meaning an image was recorded every 4 s. This is orders of magnitude  
548 higher than has been achieved before. The droplet probe had a radius of 200 nm, giving high spatial  
549 resolution too, with about 1000 pixels  $\mu\text{m}^{-2}$ . Piezo stages that have low capacity and high resonance  
550 frequency are required for imaging at these high speeds [119][113].

551 Faster imaging can result in new insights on dynamic processes, such as nanoparticle nucleation  
552 and growth. In the last five years, advances in the scanning pattern and fast response of tip-  
553 positioning has facilitated imaging with frame rates less up to 0.24 fps. In these examples, both high  
554 spatial and high temporal resolution are achieved. There are alternative strategies to increase the  
555 temporal resolution of electrochemical imaging, such as by using microelectrode arrays.

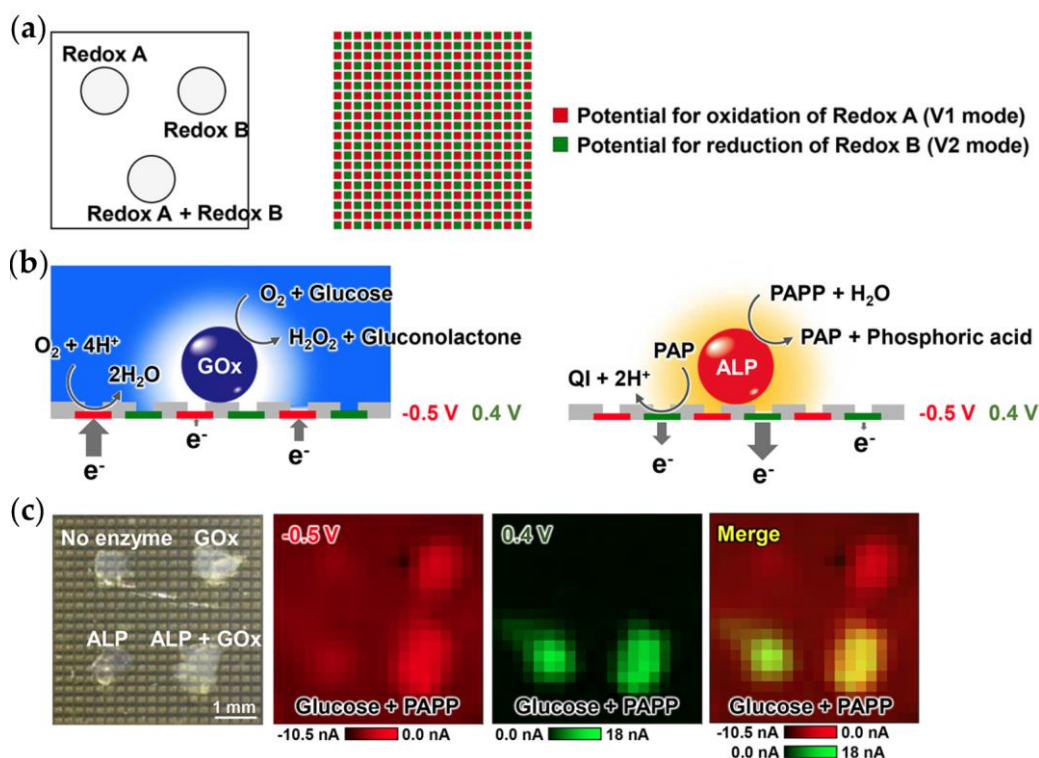
## 556 7. Microelectrode Arrays and Large-Scale Integration Chips

557 Electrochemical imaging can also be achieved without the use of a scanned probe, through the  
558 use of an individually addressable microelectrode array (MEA) or similar devices. MEAs have been  
559 presented as a means to “image” single cells, rapidly and quantitatively [120][121]. Ewing and  
560 coworkers used well-based MEAs, with  $16 \times 4 \mu\text{m}$ ,  $25 \times 3 \mu\text{m}$  or  $36 \times 2 \mu\text{m}$  square ultramicroelectrodes  
561 at a few microns separation, each in a  $40 \times 40 \mu\text{m}$  area dimensions that allowed for examining  
562 exocytosis events from a single pheochromocytoma PC12 cell [121]. Video imaging data were  
563 presented at 8-electrodes that the cell covered, showing subcellular spatial heterogeneity of exocytotic  
564 release. The devices were coated in a mouse collagen IV solution that promoted adhesion of the PC12  
565 cells, so they could grow directly over the electrode wells of the MEA. Subsequent work was carried  
566 out that deployed a movable lithographically fabricated thin film MEA, to perform 2-dimensional  
567 imaging of single vesicle release events [122], obtaining a balance between spatial resolution ( $1.2 \mu\text{m}$   
568 closely packed electrodes) and very good temporal resolution. This method relied on there being  
569 enough molecules in a single exocytosis event that they could be detected by three or more opposing  
570 electrodes, by modelling the response at these electrodes to locate the origin of exocytotic release.  
571 This was employed to distinguish heterogeneity within a single chromaffin cell surface for the release  
572 of catecholamine, stimulated by  $\text{BaCl}_2$  and  $\text{MgCl}_2$ .

573 Large-scale integration (LSI) chips, which pair a charge-coupled device (CCD) and a  
574 complementary metal-oxide semiconductor (CMOS) sensor, have been used to image biomolecule  
575 concentrations typically on a millimeter scale with pixels (sensors) 10s of  $\mu\text{m}$  across. This is a much  
576 larger scale than is generally used for SEPM imaging, bar a few exceptions [123]. This type of sensor  
577 is useful for high-throughput analysis, largely because it offers the ability to probe many samples at  
578 once, under well-defined conditions. As an imaging tool, the size of the device, and inherently needed  
579 electrode separation distance, will limit its use. Due to the limitations of device size and structure,  
580 this type of imaging will typically have lower resolution [124]. Matsue and coworkers used an  
581 amperometric sensor array device at a size-scale suited to cell clusters.

582 Matsue and coworkers have been instrumental in developing this type of imaging platform, with  
583 the most widely used application being interrogation of 3D cultured cells using electrochemical chip  
584 devices [125]. MEAs require time-consuming and sophisticated fabrication methods. Also, the  
585 interelectrode spacing is an important factor that governs spatial resolution, since electrodes need to  
586 be sufficiently separated to avoid chemical cross-talk between adjacent electrodes. To enhance the  
587 ability of the sensor array device, the approach has been extended to offer simultaneous multi-  
588 reaction imaging. In electrochemicolor imaging, two (or more) different potentials are applied at  
589 alternate electrodes within the array (Figure 7) [126]. Alternate potentials can be applied at alternate  
590 electrodes on the device (V1 and V2 modes in Figure 7), with only moderate loss of imaging spatial  
591 resolution, using a mathematical approach to fill in the now “missing” pixels. Importantly, current is  
592 measured simultaneously at all pixels, so temporal resolution is not affected. This is demonstrated  
593 for the simultaneous imaging of activities of glucose oxidase (GOx) and alkaline phosphatase (ALP)  
594 at enzyme membranes (Figure 7) as a proof of principle, and for mouse ES cell cultures (embryoid  
595 bodies). The enzymatic reaction of glucose oxidase (GOx) with glucose consumes  $\text{O}_2$ , leading to a  
596 lower measured current associated with  $\text{O}_2$  reduction at the electrode surface, which was held at a  
597 potential of  $-0.5 \text{ V}$ . Similarly, alkaline phosphatase (ALP) reacts with *p*-aminophenol phosphate  
598 (PAPP) to form *p*-aminophenol (PAP), which was measured electrochemically at the electrode surface  
599 by oxidation to *p*-quinone imine (QI), when the potential was held at  $+0.4 \text{ V}$ . These indirect  
600 measurements of non-electrochemically active species are common for biosensor platforms, and the  
601 ability to hold different potentials for different electrodes within an array partly overcomes the  
602 problem of selectivity, since it is possible to monitor multiple biomolecules simultaneously.  
603 Furthermore, images acquired using this platform show the activities associated with two molecules,  
604 using two color scales to differentiate between the electrode potential at which the current was  
605 collected.

606



607  
 608 **Figure 7.** Principles and example images using electrochemicolor imaging. (a) Schematic of a  
 609 sample over a microelectrode array that has individual alternate electrodes set at a potential to  
 610 oxidize redox species A (red) and reduce redox species B (green). (b) Schematics for the detection  
 611 mechanism of GOx activity (left) and ALP activity (right). (c) Optical microscope image (left) and  
 612 electrochemical current images (right three panels) of four membranes on the MEA device with  
 613 glucose and PAPP. (Adapted with permission from Ref [126]  
 614 (<http://pubs.acs.org/doi/10.1021/acs.analchem.7b03042>). Further permissions related to the material  
 615 excerpted should be directed to the ACS).

616  
 617  
 618  
 619  
 620  
 621  
 622  
 623  
 624  
 625

Another novel approach is integrating a MEA and microfluidic device for chemical imaging using electrochemistry. SECM is incompatible with closed microchannels, due to the requirement of a scanned probe positioned directly above the substrate. The first imaging using *in situ* voltammetry for microfluidics used a  $20 \times 10$  electrode array (Figure 8) [127]. This technique has inherently very low spatial resolution, which could be as low as  $25 \mu\text{m}$  for  $340 \times 340 \mu\text{m}$  electrodes, limited by the device fabrication. While this technique suffers poor spatial resolution as compared with SEPM, very fast temporal resolution is achieved. Moreover, this type of device further illustrates the possibility of chemical imaging in environments that SEPM is not feasible.

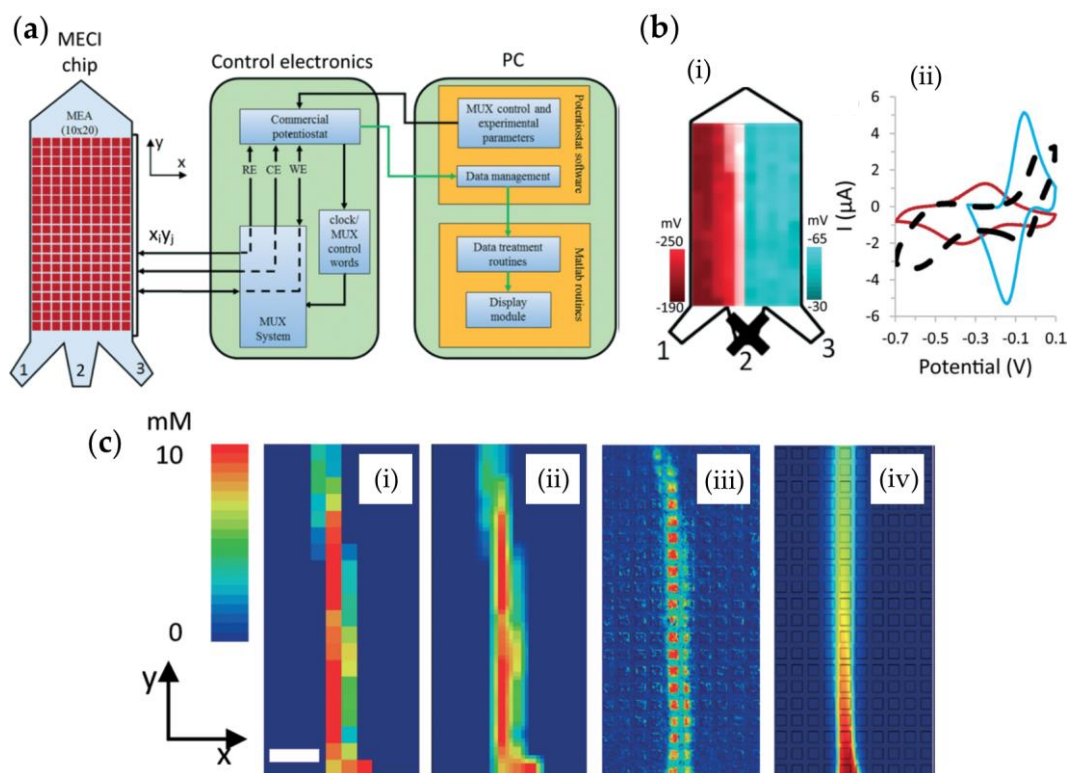


**Figure 8.** Electrochemical imaging for microfluidics. (a) Schematic of microfluidic device housing a MEA. (b) (i) Electrochemical image of a co-flow of  $\text{Ru}(\text{NH}_3)_6^{3+}$  (red) and  $\text{Fe}(\text{CN})_6^{3-}$  (blue) at inlet 1 and 3, respectively. (ii) Representative CVs for  $\text{Ru}(\text{NH}_3)_6^{3+}$  (red),  $\text{Fe}(\text{CN})_6^{3-}$  (blue) and the overlapping region (black dashed), without baseline correction. (c) Electrochemical image of 10 mM  $\text{Fe}(\text{CN})_6^{3-}$  stream from inlet 2, with confinement streams from inlets 1 and 3. (i) raw data, (ii) after smoothing algorithm applied (iii) optical image with dye added to the analyte and (iv) computer simulation. Scale bar is 1 mm. (Adapted from Ref [127] with permission of The Royal Society of Chemistry).

Using 64 subarrays of 128 individual Pt working electrodes, high-density MEAs of 8192 individually addressable electrodes were created and used to map norepinephrine across a  $2 \times 2$  mm area [128]. Temporal resolution was limited to 10 ms per subarray, or 64 seconds at a rate of 1 Hz per subarray. Spatial resolution was limited to  $30 \mu\text{m}$ . As pointed out in their work, this system should be best suited to augment traditional microscopy methods and as a tool to image chemical distributions in biological systems. In a proof-of-concept design proposed by Henry and coworkers, using only four devices (each with a  $130 \mu\text{m}$  sampling port leading to carbon paste electrodes (CPEs)), the chemical gradient of dopamine was probed across a 3 mm length scale (sampling ports positioned 1 mm apart) over hundreds of seconds (with continuous measurement of current) [129]. While this may not strictly be considered imaging (currents were only spatially resolved in one-dimension), the results serve well as an introduction to the benefits of using multiple electrode platforms for the spatiotemporal resolution of targets that do not require the use of fluorescent or chemiluminescent active targets as used in other microscopy platforms.

A promising method in the application of biosensor probes to realize a real-time spatially resolved imaging strategy is to use devices with a low-number of (multiple) electrodes over a large area [130]. As a particularly useful method for spatially resolved measurements in challenging biological systems, such as intracortical recordings, this technology is still developing [131]. It has been shown that flexible neural probes can be inserted into living tissue, with the assistance of a stiffer assembly, in a further example of an application of electrochemical imaging in a location inaccessible to standard SEPM methods operated with a mobile scanning probe [132]. Although this concept has yet to be applied to producing images of chemical concentration, different sensors for

658 multi-analyte detection (e.g. glutamate and dopamine) or for spatially resolved measurements has  
659 been achieved [133].

660 The first report of an application of a LSI-based device for real-time electrochemical-based long  
661 time (over 3 hours) monitoring of cells, was demonstrated for measuring alkaline phosphatase (ALP)  
662 from embryoid bodies [134]. Other devices have been made that are suitable for large substrate  
663 surfaces that require rapid electrochemical imaging. Topography and conductivity were measured  
664 using a LSI-based device with 400-electrode sensors to produce images of a series of large substrate  
665 surfaces [135]. Potentiometric bioimaging using the same LSI-based device was achieved by  
666 modifying the electrodes for enzyme activity measurements of glucose oxidase and ALP, at  
667 embryonic stem (ES) cells [136]. MEAs are amenable to biosensor modifications, and these devices  
668 represent a promising new tool for bioimaging of enzyme activity and chemical concentrations over  
669 large areas (mm scale). An important consideration for achieving higher resolution imaging when  
670 using MEAs is the possibility of cross-talk between adjacent electrodes, although this can be avoided  
671 if the thickness of the diffusion layer of each microelectrode is less than half the separation distance  
672 between the electrodes.

673 Lindau and coworkers showed that single vesicle release events from chromaffin cells were  
674 resolved from spikes in the current-time traces (which constituted the pixels of the electrochemical  
675 image) owing to the low pA current resolution and effective temporal resolution of 0.5 ms (giving a  
676 sensitivity of ~6000 molecules) [137]. The device comprised a 100-electrode array (10 × 10 low noise  
677 complementary metal–oxide–semiconductor (CMOS) potentiostat array) that was used to detect  
678 dopamine release.

#### 679 *7.1. Scanning Electrochemical Microscopy using Microelectrode Array Probes*

680 There are examples of combining SECM and MEAs, that involve using a linear array as a  
681 scanned probe [138][139]. Single soft probes were developed by Girault and coworkers (for  
682 antioxidant mapping) that were capable of tracing the contours of a soft surface [140]. These probes  
683 were developed into soft linear array probes, in an approach that allows scanning over a large area  
684 in a shorter time than for a single electrode probe to achieve high-throughput imaging [141]. A  
685 disadvantage of using a linear array as a scanned probe is that given a topographically varied site,  
686 each electrode will be at a slightly different tip-substrate separation distance during the scan. A  
687 means to overcome this is to use a fingerprobe (FP) MEA, in which each electrode in the array traces  
688 the topography independently of its neighboring electrodes [142], or spider-probes, which operate  
689 on the same principle [143].

## 690 **8. Conclusions and Perspectives**

691 In this review, the recent advances in chemical imaging using electrochemical methods have  
692 been summarized, with a particular focus on scanning methods that use principles of SECM and  
693 SICM for cell imaging. There has been much attention on the improvements in both spatial and  
694 temporal resolution in electrochemical imaging. With spatial resolution, smaller probes used in SEPM  
695 offer improved resolution, provided that the chemical sensing ability of electrodes at low micro- and  
696 nanoscale sizes matches those of their macroscale equivalents. With temporal resolution,  
697 improvements in SEPM have required piezoelectric positioners with a high-resonance frequency. The  
698 alternative to SEPM is to use MEA devices, although there are technical challenges that limit the  
699 spatial resolution of these platforms.

700 A future direction of electrochemical imaging will be the further integration of complementary  
701 techniques, as has been successfully achieved for SECM-AFM, SECM-SICM and most recently ICP-  
702 SICM. The integration of biosensors that offer specificity for a target of interest to SEPM is particularly  
703 exciting, since non-electrochemically active molecules may be detected using sensors with high  
704 specificity. There are further opportunities to couple electrochemical imaging platforms with other  
705 techniques, such as SECM-ATR and SECM-Raman.

706 SICM in the traditional sense does not provide chemical information, but it is a powerful tool in  
707 SEPM as a means of topography determination, and has proven useful for local delivery of molecules

708 to a substrate. SECM offers chemical imaging, especially in solutions of few interfering species,  
709 although selectivity is usually limited to redox-active molecules that can be distinguished by their  
710 sufficiently unique redox potentials. Electrochemical biosensors, ion-selective electrodes and ion  
711 channel probes offer superior selectivity, though these types of probes require additional time and  
712 care in fabrication. The field of electrochemical biosensors has thus far largely presented  
713 opportunities for point-of-care applications that employ macroscale sensors. Further applications of  
714 miniaturized sensors used in SEPM can be expected within the emerging fields of quantitative  
715 measurement of specific targets using ICPs and STING sensors for SICM and E-AB sensors for SECM.  
716

717 **Acknowledgments:** This material is based upon work supported by the National Science Foundation under  
718 CHE - 1608679.

719 **Conflicts of Interest:** The authors declare no conflict of interest.

720

721 **References**

- 722 1. Li, Y.; Ning, X.; Ma, Q.; Qin, D.; Lu, X. Recent advances in electrochemistry by scanning  
723 electrochemical microscopy. *TrAC Trends Anal. Chem.* **2016**, *80*, 242–254,  
724 doi:10.1016/j.trac.2016.02.002.
- 725 2. Zoski, C. G. Review—Advances in Scanning Electrochemical Microscopy (SECM). *J.*  
726 *Electrochem. Soc.* **2016**, *163*, H3088–H3100, doi:10.1149/2.0141604jes.
- 727 3. Izquierdo, J.; Knittel, P.; Kranz, C. Scanning electrochemical microscopy: an analytical  
728 perspective. *Anal. Bioanal. Chem.* **2018**, *410*, 307–324, doi:10.1007/s00216-017-0742-7.
- 729 4. Bergner, S.; Vatsyayan, P.; Matysik, F.-M. Recent advances in high resolution scanning  
730 electrochemical microscopy of living cells – A review. *Anal. Chim. Acta* **2013**, *775*, 1–13,  
731 doi:10.1016/j.aca.2012.12.042.
- 732 5. Schulte, A.; Nebel, M.; Schuhmann, W. Scanning Electrochemical Microscopy in  
733 Neuroscience. *Annu. Rev. Anal. Chem.* **2010**, *3*, 299–318,  
734 doi:10.1146/annurev.anchem.111808.073651.
- 735 6. Page, A.; Perry, D.; Unwin, P. R. Multifunctional scanning ion conductance microscopy. *Proc.*  
736 *R. Soc. A Math. Phys. Eng. Sci.* **2017**, *473*, doi:10.1098/rspa.2016.0889.
- 737 7. Takahashi, Y.; Kumatani, A.; Shiku, H.; Matsue, T. Scanning Probe Microscopy for Nanoscale  
738 Electrochemical Imaging. *Anal. Chem.* **2017**, *89*, 342–357, doi:10.1021/acs.analchem.6b04355.
- 739 8. Kranz, C. Recent advancements in nanoelectrodes and nanopipettes used in combined  
740 scanning electrochemical microscopy techniques. *Analyst* **2014**, *139*, 336–352,  
741 doi:10.1039/C3AN01651J.
- 742 9. Kang, M.; Momotenko, D.; Page, A.; Perry, D.; Unwin, P. R. Frontiers in Nanoscale  
743 Electrochemical Imaging: Faster, Multifunctional, and Ultrasensitive. *Langmuir* **2016**, *32*, 7993–  
744 8008, doi:10.1021/acs.langmuir.6b01932.
- 745 10. Kueng, A.; Kranz, C.; Mizaikoff, B. Scanning Probe Microscopy with Integrated Biosensors.  
746 *Sens. Lett.* **2003**, *1*, 2–15, doi:10.1166/sl.2003.001.
- 747 11. Bard, A. J.; Fan, F. R. F.; Kwak, J.; Lev, O. Scanning electrochemical microscopy. Introduction  
748 and principles. *Anal. Chem.* **1989**, *61*, 132–138, doi:10.1021/ac00177a011.
- 749 12. Heinze, J. Ultramicroelectrodes in Electrochemistry. *Angew. Chemie Int. Ed. English* **1993**, *32*,  
750 1268–1288, doi:10.1002/anie.199312681.
- 751 13. Bard, A. J.; Fan, F.-R. F.; Pierce, D. T.; Unwin, P. R.; Wipf, D. O.; Zhou, F. Chemical Imaging of  
752 Surfaces with the Scanning Electrochemical Microscope. *Science (80-. )*. **1991**, *254*, 68 LP-74,  
753 doi:10.1126/science.254.5028.68.

- 754 14. Payne, N. A.; Stephens, L. I.; Mauzeroll, J. The Application of Scanning Electrochemical  
755 Microscopy to Corrosion Research. *CORROSION* **2017**, *73*, 759–780, doi:10.5006/2354.
- 756 15. Perry, A. R.; Lazenby, R. A.; Adobes-Vidal, M.; Peruffo, M.; McKelvey, K.; Snowden, M. E.;  
757 Unwin, P. R. Hopping intermittent contact-scanning electrochemical microscopy (HIC-SECM)  
758 as a new local dissolution kinetic probe: application to salicylic acid dissolution in aqueous  
759 solution. *CrystEngComm* **2015**, *17*, 7835–7843, doi:10.1039/C5CE00138B.
- 760 16. Ishimatsu, R.; Kim, J.; Jing, P.; Striemer, C. C.; Fang, D. Z.; Fauchet, P. M.; McGrath, J. L.;  
761 Amemiya, S. Ion-Selective Permeability of an Ultrathin Nanoporous Silicon Membrane as  
762 Probed by Scanning Electrochemical Microscopy Using Micropipet-Supported ITIES Tips.  
763 *Anal. Chem.* **2010**, *82*, 7127–7134, doi:10.1021/ac1005052.
- 764 17. Oyamatsu, D.; Hirano, Y.; Kanaya, N.; Mase, Y.; Nishizawa, M.; Matsue, T. Imaging of enzyme  
765 activity by scanning electrochemical microscope equipped with a feedback control for  
766 substrate–probe distance. *Bioelectrochemistry* **2003**, *60*, 115–121, doi:10.1016/S1567-  
767 5394(03)00055-0.
- 768 18. Gyurcsányi, R. E.; Jágerszki, G.; Kiss, G.; Tóth, K. Chemical imaging of biological systems with  
769 the scanning electrochemical microscope. *Bioelectrochemistry* **2004**, *63*, 207–215,  
770 doi:10.1016/j.bioelechem.2003.12.011.
- 771 19. Kwak, J.; Bard, A. J. Scanning electrochemical microscopy. Theory of the feedback mode.  
772 *Anal. Chem.* **1989**, *61*, 1221–1227, doi:10.1021/ac00186a009.
- 773 20. D. Martin, R.; R. Unwin, P. Scanning electrochemical microscopy Kinetics of chemical  
774 reactions following electron-transfer measured with the substrate-generation-tip-collection  
775 mode. *J. Chem. Soc. Faraday Trans.* **1998**, *94*, 753–759, doi:10.1039/A707984B.
- 776 21. Eckhard, K.; Chen, X.; Turcu, F.; Schuhmann, W. Redox competition mode of scanning  
777 electrochemical microscopy (RC-SECM) for visualisation of local catalytic activity. *Phys. Chem.*  
778 *Chem. Phys.* **2006**, *8*, 5359–5365, doi:10.1039/B609511A.
- 779 22. Rodríguez-López, J.; Alpuche-Avilés, M. A.; Bard, A. J. Interrogation of Surfaces for the  
780 Quantification of Adsorbed Species on Electrodes: Oxygen on Gold and Platinum in Neutral  
781 Media. *J. Am. Chem. Soc.* **2008**, *130*, 16985–16995, doi:10.1021/ja8050553.
- 782 23. O’Connell, M. A.; Wain, A. J. Combined electrochemical-topographical imaging: a critical  
783 review. *Anal. Methods* **2015**, *7*, 6983–6999, doi:10.1039/C5AY00557D.
- 784 24. Eckhard, K.; Schuhmann, W. Alternating current techniques in scanning electrochemical  
785 microscopy (AC-SECM). *Analyst* **2008**, *133*, 1486–1497, doi:10.1039/B806721J.
- 786 25. Wipf, D. O.; Bard, A. J. Scanning electrochemical microscopy. 15. Improvements in imaging  
787 via tip-position modulation and lock-in detection. *Anal. Chem.* **1992**, *64*, 1362–1367,  
788 doi:10.1021/ac00037a011.

- 789 26. Hengstenberg, A.; Kranz, C.; Schuhmann, W. Facilitated Tip-Positioning and Applications of  
790 Non-Electrode Tips in Scanning Electrochemical Microscopy Using a Shear Force Based  
791 Constant-Distance Mode. *Chem. – A Eur. J.* **2000**, *6*, 1547–1554, doi:10.1002/(SICI)1521-  
792 3765(20000502)6:9<1547::AID-CHEM1547>3.0.CO;2-C.
- 793 27. McKelvey, K.; Edwards, M. A.; Unwin, P. R. Intermittent Contact–Scanning Electrochemical  
794 Microscopy (IC–SECM): A New Approach for Tip Positioning and Simultaneous Imaging of  
795 Interfacial Topography and Activity. *Anal. Chem.* **2010**, *82*, 6334–6337, doi:10.1021/ac101099e.
- 796 28. Sundaresan, V.; Marchuk, K.; Yu, Y.; Titus, E. J.; Wilson, A. J.; Armstrong, C. M.; Zhang, B.;  
797 Willets, K. A. Visualizing and Calculating Tip–Substrate Distance in Nanoscale Scanning  
798 Electrochemical Microscopy Using 3-Dimensional Super-Resolution Optical Imaging. *Anal.*  
799 *Chem.* **2017**, *89*, 922–928, doi:10.1021/acs.analchem.6b04073.
- 800 29. Edwards, M. A.; Whitworth, A. L.; Unwin, P. R. Quantitative Analysis and Application of Tip  
801 Position Modulation-Scanning Electrochemical Microscopy. *Anal. Chem.* **2011**, *83*, 1977–1984,  
802 doi:10.1021/ac102680v.
- 803 30. Comstock, D. J.; Elam, J. W.; Pellin, M. J.; Hersam, M. C. Integrated  
804 Ultramicroelectrode–Nanopipet Probe for Concurrent Scanning Electrochemical Microscopy  
805 and Scanning Ion Conductance Microscopy. *Anal. Chem.* **2010**, *82*, 1270–1276,  
806 doi:10.1021/ac902224q.
- 807 31. Takahashi, Y.; Shevchuk, A. I.; Novak, P.; Murakami, Y.; Shiku, H.; Korchev, Y. E.; Matsue, T.  
808 Simultaneous Noncontact Topography and Electrochemical Imaging by SECM/SICM  
809 Featuring Ion Current Feedback Regulation. *J. Am. Chem. Soc.* **2010**, *132*, 10118–10126,  
810 doi:10.1021/ja1029478.
- 811 32. Gardner, C. E.; Macpherson, J. V Peer Reviewed: Atomic Force Microscopy Probes Go  
812 Electrochemical. *Anal. Chem.* **2002**, *74*, 576 A–584 A, doi:10.1021/ac0221482.
- 813 33. Velmurugan, J.; Agrawal, A.; An, S.; Choudhary, E.; Szalai, V. A. Fabrication of Scanning  
814 Electrochemical Microscopy-Atomic Force Microscopy Probes to Image Surface Topography  
815 and Reactivity at the Nanoscale. *Anal. Chem.* **2017**, *89*, 2687–2691,  
816 doi:10.1021/acs.analchem.7b00210.
- 817 34. Seifert, J.; Rheinlaender, J.; Novak, P.; Korchev, Y. E.; Schäffer, T. E. Comparison of Atomic  
818 Force Microscopy and Scanning Ion Conductance Microscopy for Live Cell Imaging. *Langmuir*  
819 **2015**, *31*, 6807–6813, doi:10.1021/acs.langmuir.5b01124.
- 820 35. Ludwig, M.; Kranz, C.; Schuhmann, W.; Gaub, H. E. Topography feedback mechanism for the  
821 scanning electrochemical microscope based on hydrodynamic forces between tip and sample.  
822 *Rev. Sci. Instrum.* **1995**, *66*, 2857–2860, doi:10.1063/1.1145568.
- 823 36. Ballesteros Katemann, B.; Schulte, A.; Schuhmann, W. Constant-Distance Mode Scanning  
824 Electrochemical Microscopy (SECM)—Part I: Adaptation of a Non-Optical Shear-Force-Based

- 825 Positioning Mode for SECM Tips. *Chem. – A Eur. J.* **2003**, *9*, 2025–2033,  
826 doi:10.1002/chem.200204267.
- 827 37. Clausmeyer, J.; Schuhmann, W. Nanoelectrodes: Applications in electrocatalysis, single-cell  
828 analysis and high-resolution electrochemical imaging. *TrAC Trends Anal. Chem.* **2016**, *79*, 46–  
829 59, doi:10.1016/j.trac.2016.01.018.
- 830 38. Nioradze, N.; Chen, R.; Kim, J.; Shen, M.; Santhosh, P.; Amemiya, S. Origins of Nanoscale  
831 Damage to Glass-Sealed Platinum Electrodes with Submicrometer and Nanometer Size. *Anal.*  
832 *Chem.* **2013**, *85*, 6198–6202, doi:10.1021/ac401316n.
- 833 39. Chen, R.; Hu, K.; Yu, Y.; Mirkin, M. V; Amemiya, S. Focused-Ion-Beam-Milled Carbon  
834 Nanoelectrodes for Scanning Electrochemical Microscopy. *J. Electrochem. Soc.* **2016**, *163*,  
835 H3032–H3037, doi:10.1149/2.0071604jes.
- 836 40. Kim, J.; Shen, M.; Nioradze, N.; Amemiya, S. Stabilizing Nanometer Scale Tip-to-Substrate  
837 Gaps in Scanning Electrochemical Microscopy Using an Isothermal Chamber for Thermal  
838 Drift Suppression. *Anal. Chem.* **2012**, *84*, 3489–3492, doi:10.1021/ac300564g.
- 839 41. Kim, J.; Renault, C.; Nioradze, N.; Arroyo-Currás, N.; Leonard, K. C.; Bard, A. J. Nanometer  
840 Scale Scanning Electrochemical Microscopy Instrumentation. *Anal. Chem.* **2016**, *88*, 10284–  
841 10289, doi:10.1021/acs.analchem.6b03024.
- 842 42. Sun, T.; Yu, Y.; Zacher, B. J.; Mirkin, M. V Scanning Electrochemical Microscopy of Individual  
843 Catalytic Nanoparticles. *Angew. Chemie Int. Ed.* **2014**, *53*, 14120–14123,  
844 doi:10.1002/anie.201408408.
- 845 43. Kim, J.; Renault, C.; Nioradze, N.; Arroyo-Currás, N.; Leonard, K. C.; Bard, A. J.  
846 Electrocatalytic Activity of Individual Pt Nanoparticles Studied by Nanoscale Scanning  
847 Electrochemical Microscopy. *J. Am. Chem. Soc.* **2016**, *138*, 8560–8568, doi:10.1021/jacs.6b03980.
- 848 44. Chen, R.; Balla, R. J.; Lima, A.; Amemiya, S. Characterization of Nanopipet-Supported ITIES  
849 Tips for Scanning Electrochemical Microscopy of Single Solid-State Nanopores. *Anal. Chem.*  
850 **2017**, *89*, 9946–9952, doi:10.1021/acs.analchem.7b02269.
- 851 45. Wang, Y.; Kececi, K.; Velmurugan, J.; Mirkin, M. V Electron transfer/ion transfer mode of  
852 scanning electrochemical microscopy (SECM): a new tool for imaging and kinetic studies.  
853 *Chem. Sci.* **2013**, *4*, 3606–3616, doi:10.1039/C3SC50825K.
- 854 46. Hansma, P. K.; Drake, B.; Marti, O.; Gould, S. A.; Prater, C. B. The scanning ion-conductance  
855 microscope. *Science (80-. )*. **1989**, *243*, 641 LP-643, doi:10.1126/science.2464851.
- 856 47. Rheinlaender, J.; Schäffer, T. E. Lateral Resolution and Image Formation in Scanning Ion  
857 Conductance Microscopy. *Anal. Chem.* **2015**, *87*, 7117–7124, doi:10.1021/acs.analchem.5b00900.
- 858 48. Nakajima, M.; Mizutani, Y.; Iwata, F.; Ushiki, T. Scanning ion conductance microscopy for  
859 visualizing the three-dimensional surface topography of cells and tissues. *Semin. Cell Dev. Biol.*

- 860           **2018**, *73*, 125–131, doi:10.1016/j.semcd.2017.09.024.
- 861   49.   Momotenko, D.; McKelvey, K.; Kang, M.; Meloni, G. N.; Unwin, P. R. Simultaneous Interfacial  
862        Reactivity and Topography Mapping with Scanning Ion Conductance Microscopy. *Anal.*  
863        *Chem.* **2016**, *88*, 2838–2846, doi:10.1021/acs.analchem.5b04566.
- 864   50.   McKelvey, K.; Perry, D.; Byers, J. C.; Colburn, A. W.; Unwin, P. R. Bias Modulated Scanning  
865        Ion Conductance Microscopy. *Anal. Chem.* **2014**, *86*, 3639–3646, doi:10.1021/ac5003118.
- 866   51.   Chen, C.-C.; Baker, L. A. Effects of pipette modulation and imaging distances on ion currents  
867        measured with Scanning Ion Conductance Microscopy (SICM). *Analyst* **2011**, *136*, 90–97,  
868        doi:10.1039/C0AN00604A.
- 869   52.   Perry, D.; Page, A.; Chen, B.; Frenguelli, B. G.; Unwin, P. R. Differential-Concentration  
870        Scanning Ion Conductance Microscopy. *Anal. Chem.* **2017**, *89*, 12458–12465,  
871        doi:10.1021/acs.analchem.7b03543.
- 872   53.   Thakar, R.; Weber, A. E.; Morris, C. A.; Baker, L. A. Multifunctional carbon nanoelectrodes  
873        fabricated by focused ion beam milling. *Analyst* **2013**, *138*, 5973–5982,  
874        doi:10.1039/C3AN01216F.
- 875   54.   Lazenby, R. A.; McKelvey, K.; Peruffo, M.; Baghdadi, M.; Unwin, P. R. Nanoscale intermittent  
876        contact-scanning electrochemical microscopy. *J. Solid State Electrochem.* **2013**, *17*, 2979–2987.
- 877   55.   Takahashi, Y.; Shevchuk, A. I.; Novak, P.; Zhang, Y.; Ebejer, N.; Macpherson, J. V.; Unwin, P.  
878        R.; Pollard, A. J.; Roy, D.; Clifford, C. A.; Shiku, H.; Matsue, T.; Klenerman, D.; Korchev, Y. E.  
879        Multifunctional Nanoprobes for Nanoscale Chemical Imaging and Localized Chemical  
880        Delivery at Surfaces and Interfaces. *Angew. Chemie Int. Ed.* **2011**, *50*, 9638–9642,  
881        doi:10.1002/anie.201102796.
- 882   56.   Shi, W.; Sa, N.; Thakar, R.; Baker, L. A. Nanopipette delivery: influence of surface charge.  
883        *Analyst* **2015**, *140*, 4835–4842, doi:10.1039/C4AN01073F.
- 884   57.   Page, A.; Kang, M.; Armitstead, A.; Perry, D.; Unwin, P. R. Quantitative Visualization of  
885        Molecular Delivery and Uptake at Living Cells with Self-Referencing Scanning Ion  
886        Conductance Microscopy-Scanning Electrochemical Microscopy. *Anal. Chem.* **2017**, *89*, 3021–  
887        3028, doi:10.1021/acs.analchem.6b04629.
- 888   58.   Perry, D.; Momotenko, D.; Lazenby, R. A.; Kang, M.; Unwin, P. R. Characterization of  
889        Nanopipettes. *Anal. Chem.* **2016**, doi:10.1021/acs.analchem.6b01095.
- 890   59.   Tognoni, E.; Baschieri, P.; Ascoli, C.; Pellegrini, M.; Pellegrino, M. Characterization of tip size  
891        and geometry of the pipettes used in scanning ion conductance microscopy. *Micron* **2016**, *83*,  
892        11–18, doi:10.1016/j.micron.2016.01.002.
- 893   60.   Actis, P.; Tokar, S.; Clausmeyer, J.; Babakinejad, B.; Mikhaleva, S.; Cornut, R.; Takahashi, Y.;  
894        López Córdoba, A.; Novak, P.; Shevchuk, A. I.; Dougan, J. A.; Kazarian, S. G.; Gorelkin, P. V;

- 895 Erofeev, A. S.; Yaminsky, I. V.; Unwin, P. R.; Schuhmann, W.; Klenerman, D.; Rusakov, D. A.;  
896 Sviderskaya, E. V.; Korchev, Y. E. Electrochemical Nanoprobes for Single-Cell Analysis. *ACS*  
897 *Nano* **2014**, *8*, 875–884, doi:10.1021/nn405612q.
- 898 61. Hu, K.; Gao, Y.; Wang, Y.; Yu, Y.; Zhao, X.; Rotenberg, S. A.; Gökmeşe, E.; Mirkin, M. V.;  
899 Friedman, G.; Gogotsi, Y. Platinized carbon nanoelectrodes as potentiometric and  
900 amperometric SECM probes. *J. Solid State Electrochem.* **2013**, *17*, 2971–2977, doi:10.1007/s10008-  
901 013-2173-5.
- 902 62. O'Connell, M. A.; Lewis, J. R.; Wain, A. J. Electrochemical imaging of hydrogen peroxide  
903 generation at individual gold nanoparticles. *Chem. Commun.* **2015**, *51*, 10314–10317,  
904 doi:10.1039/C5CC01640A.
- 905 63. Şen, M.; Takahashi, Y.; Matsumae, Y.; Horiguchi, Y.; Kumatani, A.; Ino, K.; Shiku, H.; Matsue,  
906 T. Improving the Electrochemical Imaging Sensitivity of Scanning Electrochemical  
907 Microscopy-Scanning Ion Conductance Microscopy by Using Electrochemical Pt Deposition.  
908 *Anal. Chem.* **2015**, *87*, 3484–3489, doi:10.1021/acs.analchem.5b00027.
- 909 64. Justino, C. I. L.; Rocha-Santos, T. A.; Duarte, A. C.; Rocha-Santos, T. A. Review of analytical  
910 figures of merit of sensors and biosensors in clinical applications. *TrAC Trends Anal. Chem.*  
911 **2010**, *29*, 1172–1183, doi:10.1016/j.trac.2010.07.008.
- 912 65. Ganesana, M.; Lee, S. T.; Wang, Y.; Venton, B. J. Analytical Techniques in Neuroscience:  
913 Recent Advances in Imaging, Separation, and Electrochemical Methods. *Anal. Chem.* **2017**, *89*,  
914 314–341, doi:10.1021/acs.analchem.6b04278.
- 915 66. Huffman, M. L.; Venton, B. J. Carbon-Fiber Microelectrodes for In Vivo Applications. *Analyst*  
916 **2009**, *134*, 18–24, doi:10.1039/b807563h.
- 917 67. Ha, Y.; Myung, D.; Shim, J. H.; Kim, M. H.; Lee, Y. A dual electrochemical microsensor for  
918 simultaneous imaging of oxygen and pH over the rat kidney surface. *Analyst* **2013**, *138*, 5258–  
919 5264, doi:10.1039/C3AN00878A.
- 920 68. Nadappuram, B. P.; McKelvey, K.; Al Botros, R.; Colburn, A. W.; Unwin, P. R. Fabrication and  
921 Characterization of Dual Function Nanoscale pH-Scanning Ion Conductance Microscopy  
922 (SICM) Probes for High Resolution pH Mapping. *Anal. Chem.* **2013**, *85*, 8070–8074,  
923 doi:10.1021/ac401883n.
- 924 69. Lin, T.-E.; Cortés-Salazar, F.; Lesch, A.; Qiao, L.; Bondarenko, A.; Girault, H. H. Multiple  
925 scanning electrochemical microscopy mapping of tyrosinase in micro-contact printed fruit  
926 samples on polyvinylidene fluoride membrane. *Electrochim. Acta* **2015**, *179*, 57–64,  
927 doi:10.1016/j.electacta.2015.03.224.
- 928 70. Horrocks, B. R.; Schmidtke, D.; Heller, A.; Bard, A. J. Scanning electrochemical microscopy.  
929 24. Enzyme ultramicroelectrodes for the measurement of hydrogen peroxide at surfaces. *Anal.*  
930 *Chem.* **1993**, *65*, 3605–3614, doi:10.1021/ac00072a013.

- 931 71. Polcari, D.; Kwan, A.; Van Horn, M. R.; Danis, L.; Pollegioni, L.; Ruthazer, E. S.; Mauzeroll, J.  
932 Disk-Shaped Amperometric Enzymatic Biosensor for in Vivo Detection of d-serine. *Anal.*  
933 *Chem.* **2014**, *86*, 3501–3507, doi:10.1021/ac404111u.
- 934 72. Polcari, D.; Perry, S. C.; Pollegioni, L.; Geissler, M.; Mauzeroll, J. Localized Detection of d-  
935 Serine by using an Enzymatic Amperometric Biosensor and Scanning Electrochemical  
936 Microscopy. *ChemElectroChem* **2017**, *4*, 920–926, doi:10.1002/celec.201600766.
- 937 73. Ciobanu, M.; Taylor, D. E.; Wilburn, J. P.; Cliffel, D. E. Glucose and Lactate Biosensors for  
938 Scanning Electrochemical Microscopy Imaging of Single Live Cells. *Anal. Chem.* **2008**, *80*,  
939 2717–2727, doi:10.1021/ac7021184.
- 940 74. Lugo-Morales, L. Z.; Loziuk, P. L.; Corder, A. K.; Toups, J. V.; Roberts, J. G.; McCaffrey, K. A.;  
941 Sombers, L. A. Enzyme-Modified Carbon-Fiber Microelectrode for the Quantification of  
942 Dynamic Fluctuations of Nonelectroactive Analytes Using Fast-Scan Cyclic Voltammetry.  
943 *Anal. Chem.* **2013**, *85*, 8780–8786, doi:10.1021/ac4017852.
- 944 75. Soldà, A.; Valenti, G.; Marcaccio, M.; Giorgio, M.; Pelicci, P. G.; Paolucci, F.; Rapino, S. Glucose  
945 and Lactate Miniaturized Biosensors for SECM-Based High-Spatial Resolution Analysis: A  
946 Comparative Study. *ACS Sensors* **2017**, *2*, 1310–1318, doi:10.1021/acssensors.7b00324.
- 947 76. Creager, S. E.; Olsen, K. G. Self-assembled monolayers and enzyme electrodes: Progress,  
948 problems and prospects. *Anal. Chim. Acta* **1995**, *307*, 277–289, doi:10.1016/0003-2670(94)00506-  
949 H.
- 950 77. Zhao, F.; Conzuelo, F.; Hartmann, V.; Li, H.; Stapf, S.; Nowaczyk, M. M.; Rögner, M.; Plumeré,  
951 N.; Lubitz, W.; Schuhmann, W. A novel versatile microbiosensor for local hydrogen detection  
952 by means of scanning photoelectrochemical microscopy. *Biosens. Bioelectron.* **2017**, *94*, 433–437,  
953 doi:10.1016/j.bios.2017.03.037.
- 954 78. Wilburn, J. P.; Ciobanu, M.; Cliffel, D. E. Scanning Electrochemical Microscopy of Individual  
955 Pancreatic Islets. *J. Electrochem. Soc.* **2016**, *163*, H3077–H3082, doi:10.1149/2.0111604jes.
- 956 79. Das, J.; Kelley, S. O. Tuning the Bacterial Detection Sensitivity of Nanostructured  
957 Microelectrodes. *Anal. Chem.* **2013**, *85*, 7333–7338, doi:10.1021/ac401221f.
- 958 80. Liu, J.; Wagan, S.; Dávila Morris, M.; Taylor, J.; White, R. J. Achieving Reproducible  
959 Performance of Electrochemical, Folding Aptamer-Based Sensors on Microelectrodes:  
960 Challenges and Prospects. *Anal. Chem.* **2014**, *86*, 11417–11424, doi:10.1021/ac503407e.
- 961 81. Salamifar, S. E.; Lai, R. Y. Fabrication of Electrochemical DNA Sensors on Gold-Modified  
962 Recessed Platinum Nanoelectrodes. *Anal. Chem.* **2014**, *86*, 2849–2852, doi:10.1021/ac403816h.
- 963 82. Wang, D.; Xiao, X.; Xu, S.; Liu, Y.; Li, Y. Electrochemical aptamer-based nanosensor fabricated  
964 on single Au nanowire electrodes for adenosine triphosphate assay. *Biosens. Bioelectron.* **2018**,  
965 *99*, 431–437, doi:10.1016/j.bios.2017.08.020.

- 966 83. Wei, C.; Bard, A. J.; Nagy, G.; Toth, K. Scanning Electrochemical Microscopy. 28. Ion-Selective  
967 Neutral Carrier-Based Microelectrode Potentiometry. *Anal. Chem.* **1995**, *67*, 1346–1356,  
968 doi:10.1021/ac00104a008.
- 969 84. Izquierdo, J.; Kiss, A.; Santana, J. J.; Nagy, L.; Bitter, I.; Isaacs, H. S.; Nagy, G.; Souto, R. M.  
970 Development of Mg<sup>2+</sup> Ion-Selective Microelectrodes for Potentiometric Scanning  
971 Electrochemical Microscopy Monitoring of Galvanic Corrosion Processes. *J. Electrochem. Soc.*  
972 **2013**, *160*, C451–C459, doi:10.1149/2.001310jes.
- 973 85. Ummadi, J. G.; Downs, C. J.; Joshi, V. S.; Ferracane, J. L.; Koley, D. Carbon-Based Solid-State  
974 Calcium Ion-Selective Microelectrode and Scanning Electrochemical Microscopy: A  
975 Quantitative Study of pH-Dependent Release of Calcium Ions from Bioactive Glass. *Anal.*  
976 *Chem.* **2016**, *88*, 3218–3226, doi:10.1021/acs.analchem.5b04614.
- 977 86. Filotás, D.; Asserghine, A.; Nagy, L.; Nagy, G. Short-term influence of interfering ion activity  
978 change on ion-selective micropipette electrode potential; another factor that can affect the time  
979 needed for imaging in potentiometric SECM. *Electrochem. commun.* **2017**, *77*, 62–64,  
980 doi:10.1016/j.elecom.2017.02.010.
- 981 87. Kiss, A.; Nagy, G. Deconvolution of potentiometric SECM images recorded with high scan  
982 rate. *Electrochim. Acta* **2015**, *163*, 303–309, doi:10.1016/j.electacta.2015.02.096.
- 983 88. Yamada, H.; Haraguchi, D.; Yasunaga, K. Fabrication and Characterization of a K<sup>+</sup>-Selective  
984 Nanoelectrode and Simultaneous Imaging of Topography and Local K<sup>+</sup> Flux Using Scanning  
985 Electrochemical Microscopy. *Anal. Chem.* **2014**, *86*, 8547–8552, doi:10.1021/ac502444y.
- 986 89. Nascimento, R. A. S.; Özel, R. E.; Mak, W. H.; Mulato, M.; Singaram, B.; Pourmand, N. Single  
987 Cell “Glucose Nanosensor” Verifies Elevated Glucose Levels in Individual Cancer Cells. *Nano*  
988 *Lett.* **2016**, *16*, 1194–1200, doi:10.1021/acs.nanolett.5b04495.
- 989 90. Viložny, B.; Actis, P.; Seger, R. A.; Vallmajo-Martin, Q.; Pourmand, N. Reversible Cation  
990 Response with a Protein-Modified Nanopipette. *Anal. Chem.* **2011**, *83*, 6121–6126,  
991 doi:10.1021/ac201322v.
- 992 91. Actis, P.; Mak, A. C.; Pourmand, N. Functionalized nanopipettes: toward label-free, single cell  
993 biosensors. *Bioanal. Rev.* **2010**, *1*, 177–185, doi:10.1007/s12566-010-0013-y.
- 994 92. Umehara, S.; Karhanek, M.; Davis, R. W.; Pourmand, N. Label-free biosensing with  
995 functionalized nanopipette probes. *Proc. Natl. Acad. Sci.* **2009**, *106*, 4611 LP-4616.
- 996 93. Actis, P.; Rogers, A.; Nivala, J.; Viložny, B.; Seger, R. A.; Jejelowo, O.; Pourmand, N. Reversible  
997 thrombin detection by aptamer functionalized STING sensors. *Biosens. Bioelectron.* **2011**, *26*,  
998 4503–4507, doi:10.1016/j.bios.2011.05.010.
- 999 94. Shi, W.; Friedman, A. K.; Baker, L. A. Nanopore Sensing. *Anal. Chem.* **2017**, *89*, 157–188,  
1000 doi:10.1021/acs.analchem.6b04260.

- 1001 95. Coronado, R.; Latorre, R. Phospholipid bilayers made from monolayers on patch-clamp  
1002 pipettes. *Biophys. J.* **1983**, *43*, 231–236, doi:10.1016/S0006-3495(83)84343-4.
- 1003 96. Alvarez, O. Ion Channel Reconstitution. In *Ion Channel Reconstitution*; Miller, C., Ed.; Springer  
1004 US: New York, 1986; pp. 115–130 ISBN 978-1-4757-1363-3.
- 1005 97. Zhou, Y.; Bright, L. K.; Shi, W.; Aspinwall, C. A.; Baker, L. A. Ion Channel Probes for Scanning  
1006 Ion Conductance Microscopy. *Langmuir* **2014**, *30*, 15351–15355, doi:10.1021/la504097f.
- 1007 98. Macazo, F. C.; White, R. J. Bioinspired Protein Channel-Based Scanning Ion Conductance  
1008 Microscopy (Bio-SICM) for Simultaneous Conductance and Specific Molecular Imaging. *J.*  
1009 *Am. Chem. Soc.* **2016**, *138*, 2793–2801, doi:10.1021/jacs.5b13252.
- 1010 99. Shi, W.; Zeng, Y.; Zhou, L.; Xiao, Y.; Cummins, T. R.; Baker, L. A. Membrane patches as ion  
1011 channel probes for scanning ion conductance microscopy. *Faraday Discuss.* **2016**, *193*, 81–97,  
1012 doi:10.1039/C6FD00133E.
- 1013 100. Lazenby, R. A.; Macazo, F. C.; Wormsbecher, R. F.; White, R. J. Quantitative Framework for  
1014 Stochastic Nanopore Sensors Using Multiple Channels. *Anal. Chem.* **2018**, *90*, 903–911,  
1015 doi:10.1021/acs.analchem.7b03845.
- 1016 101. Bayley, H.; Braha, O.; Gu, L. Q. Stochastic sensing with protein pores. *Adv. Mater.* **2000**, *12*,  
1017 139–142, doi:10.1002/(SICI)1521-4095(200001)12:2<139::AID-ADMA139>3.0.CO;2-Q.
- 1018 102. Shi, W.; Zeng, Y.; Zhu, C.; Xiao, Y.; Cummins, T. R.; Hou, J.; Baker, L. A. Characterization of  
1019 Membrane Patch-Ion Channel Probes for Scanning Ion Conductance Microscopy. *Small* **2017**,  
1020 n/a-n/a, doi:10.1002/smll.201702945.
- 1021 103. Macazo, F. C.; White, R. J. Monitoring Charge Flux to Quantify Unusual Ligand-Induced Ion  
1022 Channel Activity for Use in Biological Nanopore-Based Sensors. *Anal. Chem.* **2014**, *86*, 5519–  
1023 5525, doi:10.1021/ac500832a.
- 1024 104. Novak, P.; Li, C.; Shevchuk, A. I.; Stepanyan, R.; Caldwell, M.; Hughes, S.; Smart, T. G.;  
1025 Gorelik, J.; Ostanin, V. P.; Lab, M. J.; Moss, G. W. J.; Frolenkov, G. I.; Klenerman, D.; Korchev,  
1026 Y. E. Nanoscale live-cell imaging using hopping probe ion conductance microscopy. *Nat.*  
1027 *Methods* **2009**, *6*, 279.
- 1028 105. Lazenby, R. A.; McKelvey, K.; Unwin, P. R. Hopping intermittent contact-scanning  
1029 electrochemical microscopy (HIC-SECM): Visualizing interfacial reactions and fluxes from  
1030 surfaces to bulk solution. *Anal. Chem.* **2013**, *85*, 2937–2944.
- 1031 106. Nebel, M.; Eckhard, K.; Erichsen, T.; Schulte, A.; Schuhmann, W. 4D Shearforce-Based  
1032 Constant-Distance Mode Scanning Electrochemical Microscopy. *Anal. Chem.* **2010**, *82*, 7842–  
1033 7848, doi:10.1021/ac1008805.
- 1034 107. Li, M. S. M.; Filice, F. P.; Ding, Z. Determining live cell topography by scanning  
1035 electrochemical microscopy. *J. Electroanal. Chem.* **2016**, *779*, 176–186,

- 1036 doi:10.1016/j.jelechem.2016.02.042.
- 1037 108. Filice, F. P.; Li, M. S. M.; Henderson, J. D.; Ding, Z. Mapping Cd<sup>2+</sup>-induced membrane  
1038 permeability changes of single live cells by means of scanning electrochemical microscopy.  
1039 *Anal. Chim. Acta* **2016**, *908*, 85–94, doi:10.1016/j.aca.2015.12.027.
- 1040 109. Henderson, J. D.; Filice, F. P.; Li, M. S. M.; Ding, Z. Tracking live cell response to cadmium (II)  
1041 concentrations by scanning electrochemical microscopy. *J. Inorg. Biochem.* **2016**, *158*, 92–98,  
1042 doi:10.1016/j.jinorgbio.2015.11.016.
- 1043 110. Kuss, S.; Trinh, D.; Mauzeroll, J. High-Speed Scanning Electrochemical Microscopy Method  
1044 for Substrate Kinetic Determination: Application to Live Cell Imaging in Human Cancer. *Anal.*  
1045 *Chem.* **2015**, *87*, 8102–8106, doi:10.1021/acs.analchem.5b01269.
- 1046 111. Kuss, S.; Trinh, D.; Danis, L.; Mauzeroll, J. High-Speed Scanning Electrochemical Microscopy  
1047 Method for Substrate Kinetic Determination: Method and Theory. *Anal. Chem.* **2015**, *87*, 8096–  
1048 8101, doi:10.1021/acs.analchem.5b01268.
- 1049 112. Kuss, S.; Kuss, C.; Trinh, D.; Schougaard, S. B.; Mauzeroll, J. Forced convection during  
1050 scanning electrochemical microscopy imaging over living cells: Effect of topographies and  
1051 kinetics on the microelectrode current. *Electrochim. Acta* **2013**, *110*, 42–48,  
1052 doi:10.1016/j.electacta.2013.03.149.
- 1053 113. Ida, H.; Takahashi, Y.; Kumatani, A.; Shiku, H.; Matsue, T. High Speed Scanning Ion  
1054 Conductance Microscopy for Quantitative Analysis of Nanoscale Dynamics of Microvilli.  
1055 *Anal. Chem.* **2017**, *89*, 6015–6020, doi:10.1021/acs.analchem.7b00584.
- 1056 114. Kiss, A.; Nagy, G. New SECM scanning algorithms for improved potentiometric imaging of  
1057 circularly symmetric targets. *Electrochim. Acta* **2014**, *119*, 169–174,  
1058 doi:10.1016/j.electacta.2013.12.041.
- 1059 115. Zhuang, J.; Jiao, Y.; Mugabo, V. A new scanning mode to improve scanning ion conductance  
1060 microscopy imaging rate with pipette predicted movement. *Micron* **2017**, *101*, 177–185,  
1061 doi:10.1016/j.micron.2017.07.007.
- 1062 116. Ebejer, N.; Schnippering, M.; Colburn, A. W.; Edwards, M. A.; Unwin, P. R. Localized High  
1063 Resolution Electrochemistry and Multifunctional Imaging: Scanning Electrochemical Cell  
1064 Microscopy. *Anal. Chem.* **2010**, *82*, 9141–9145, doi:10.1021/ac102191u.
- 1065 117. Bentley, C. L.; Kang, M.; Unwin, P. R. Nanoscale Structure Dynamics within Electrocatalytic  
1066 Materials. *J. Am. Chem. Soc.* **2017**, *139*, 16813–16821, doi:10.1021/jacs.7b09355.
- 1067 118. Bentley, C. L.; Kang, M.; Maddar, F. M.; Li, F.; Walker, M.; Zhang, J.; Unwin, P. R.  
1068 Electrochemical maps and movies of the hydrogen evolution reaction on natural crystals of  
1069 molybdenite (MoS<sub>2</sub>): basal vs. edge plane activity. *Chem. Sci.* **2017**, *8*, 6583–6593,  
1070 doi:10.1039/C7SC02545A.

- 1071 119. Momotenko, D.; Byers, J. C.; McKelvey, K.; Kang, M.; Unwin, P. R. High-Speed  
1072 Electrochemical Imaging. *ACS Nano* **2015**, *9*, 8942–8952, doi:10.1021/acsnano.5b02792.
- 1073 120. Wang, J.; Trouillon, R.; Lin, Y.; Svensson, M. I.; Ewing, A. G. Individually Addressable Thin-  
1074 Film Ultramicroelectrode Array for Spatial Measurements of Single Vesicle Release. *Anal.*  
1075 *Chem.* **2013**, *85*, 5600–5608, doi:10.1021/ac4009385.
- 1076 121. Wang, J.; Trouillon, R.; Dunevall, J.; Ewing, A. G. Spatial Resolution of Single-Cell Exocytosis  
1077 by Microwell-Based Individually Addressable Thin Film Ultramicroelectrode Arrays. *Anal.*  
1078 *Chem.* **2014**, *86*, 4515–4520, doi:10.1021/ac500443q.
- 1079 122. Wigström, J.; Dunevall, J.; Najafinobar, N.; Lovrić, J.; Wang, J.; Ewing, A. G.; Cans, A.-S.  
1080 Lithographic Microfabrication of a 16-Electrode Array on a Probe Tip for High Spatial  
1081 Resolution Electrochemical Localization of Exocytosis. *Anal. Chem.* **2016**, *88*, 2080–2087,  
1082 doi:10.1021/acs.analchem.5b03316.
- 1083 123. Schierbaum, N.; Hack, M.; Betz, O.; Schäffer, T. E. Macro-SICM: A Scanning Ion Conductance  
1084 Microscope for Large-Range Imaging. *Anal. Chem.* **2018**, doi:10.1021/acs.analchem.7b04764.
- 1085 124. Abe, H.; Ino, K.; Li, C.-Z.; Kanno, Y.; Inoue, K. Y.; Suda, A.; Kunikata, R.; Matsudaira, M.;  
1086 Takahashi, Y.; Shiku, H.; Matsue, T. Electrochemical Imaging of Dopamine Release from  
1087 Three-Dimensional-Cultured PC12 Cells Using Large-Scale Integration-Based Amperometric  
1088 Sensors. *Anal. Chem.* **2015**, *87*, 6364–6370, doi:10.1021/acs.analchem.5b01307.
- 1089 125. Ino, K.; Sen, M.; Shiku, H.; Matsue, T. Micro/nano-electrochemical probe and chip devices for  
1090 evaluation of three-dimensional cultured cells. *Analyst* **2017**, *142*, 4343–4354,  
1091 doi:10.1039/C7AN01442B.
- 1092 126. Kanno, Y.; Ino, K.; Abe, H.; Sakamoto, C.; Onodera, T.; Inoue, K. Y.; Suda, A.; Kunikata, R.;  
1093 Matsudaira, M.; Shiku, H.; Matsue, T. Electrochemicolor Imaging Using an LSI-Based Device  
1094 for Multiplexed Cell Assays. *Anal. Chem.* **2017**, *89*, 12778–12786,  
1095 doi:10.1021/acs.analchem.7b03042.
- 1096 127. Kara, A.; Reitz, A.; Mathault, J.; Mehrou-Loko, S.; Amirdehi, M. A.; Miled, A.; Greener, J.  
1097 Electrochemical imaging for microfluidics: a full-system approach. *Lab Chip* **2016**, *16*, 1081–  
1098 1087, doi:10.1039/C6LC00077K.
- 1099 128. Wydallis, J. B.; Feeny, R. M.; Wilson, W.; Kern, T.; Chen, T.; Tobet, S.; Reynolds, M. M.; Henry,  
1100 C. S. Spatiotemporal norepinephrine mapping using a high-density CMOS microelectrode  
1101 array. *Lab Chip* **2015**, *15*, 4075–4082, doi:10.1039/C5LC00778J.
- 1102 129. Mensack, M. M.; Wydallis, J. B.; Lynn, N. S.; Dandy, D. S.; Henry, C. S. Spatially resolved  
1103 electrochemical sensing of chemical gradients. *Lab Chip* **2013**, *13*, 208–211,  
1104 doi:10.1039/C2LC41054K.
- 1105 130. Chung, J. E.; Joo, H. R.; Fan, J. L.; Liu, D. F.; Barnett, A. H.; Chen, S.; Geaghan-Breiner, C.;

- 1106 Karlsson, M. P.; Karlsson, M.; Lee, K. Y.; Liang, H.; Magland, J. F.; Mehaffey, W. H.; Tooker,  
1107 A. C.; Brainard, M. S.; Greengard, L. F.; Tolosa, V. M.; Frank, L. M. A polymer probe-based  
1108 system for high density, long-lasting electrophysiological recordings across distributed  
1109 neuronal circuits. *bioRxiv* **2018**, doi:10.1101/242693.
- 1110 131. Szostak, K. M.; Grand, L.; Constandinou, T. G. Neural Interfaces for Intracortical Recording:  
1111 Requirements, Fabrication Methods, and Characteristics. *Front. Neurosci.* **2017**, *11*, 665.
- 1112 132. Felix, S. H.; Shah, K. G.; Tolosa, V. M.; Sheth, H. J.; Tooker, A. C.; Delima, T. L.; Jadhav, S. P.;  
1113 Frank, L. M.; Pannu, S. S. Insertion of Flexible Neural Probes Using Rigid Stiffeners Attached  
1114 with Biodissolvable Adhesive. *J. Vis. Exp.* **2013**, 50609, doi:10.3791/50609.
- 1115 133. Tseng, T. T.-C.; Monbouquette, H. G. Implantable microprobe with arrayed microsensors for  
1116 combined amperometric monitoring of the neurotransmitters, glutamate and dopamine. *J.*  
1117 *Electroanal. Chem.* **2012**, *682*, 141–146, doi:10.1016/j.jelechem.2012.07.014.
- 1118 134. Şen, M.; Ino, K.; Inoue, K. Y.; Arai, T.; Nishijo, T.; Suda, A.; Kunikata, R.; Shiku, H.; Matsue, T.  
1119 LSI-based amperometric sensor for real-time monitoring of embryoid bodies. *Biosens.*  
1120 *Bioelectron.* **2013**, *48*, 12–18, doi:10.1016/j.bios.2013.03.069.
- 1121 135. Kanno, Y.; Ino, K.; Inoue, K. Y.; Şen, M.; Suda, A.; Kunikata, R.; Matsudaira, M.; Abe, H.; Li,  
1122 C.-Z.; Shiku, H.; Matsue, T. Feedback mode-based electrochemical imaging of conductivity  
1123 and topography for large substrate surfaces using an LSI-based amperometric chip device  
1124 with 400 sensors. *J. Electroanal. Chem.* **2015**, *741*, 109–113, doi:10.1016/j.jelechem.2015.01.020.
- 1125 136. Kanno, Y.; Ino, K.; Sakamoto, C.; Inoue, K. Y.; Matsudaira, M.; Suda, A.; Kunikata, R.;  
1126 Ishikawa, T.; Abe, H.; Shiku, H.; Matsue, T. Potentiometric bioimaging with a large-scale  
1127 integration (LSI)-based electrochemical device for detection of enzyme activity. *Biosens.*  
1128 *Bioelectron.* **2016**, *77*, 709–714, doi:10.1016/j.bios.2015.10.021.
- 1129 137. Kim, B. N.; Herbst, A. D.; Kim, S. J.; Minch, B. A.; Lindau, M. Parallel recording of  
1130 neurotransmitters release from chromaffin cells using a 10×10 CMOS IC potentiostat array  
1131 with on-chip working electrodes. *Biosens. Bioelectron.* **2013**, *41*, 736–744,  
1132 doi:10.1016/j.bios.2012.09.058.
- 1133 138. Barker, A. L.; Unwin, P. R.; Gardner, J. W.; Rieley, H. A multi-electrode probe for parallel  
1134 imaging in scanning electrochemical microscopy. *Electrochem. commun.* **2004**, *6*, 91–97,  
1135 doi:10.1016/j.elecom.2003.10.019.
- 1136 139. Cortés-Salazar, F.; Momotenko, D.; Girault, H. H.; Lesch, A.; Wittstock, G. Seeing Big with  
1137 Scanning Electrochemical Microscopy. *Anal. Chem.* **2011**, *83*, 1493–1499,  
1138 doi:10.1021/ac101931d.
- 1139 140. Lin, T.-E.; Lesch, A.; Li, C.-L.; Girault, H. H. Mapping the antioxidant activity of apple peels  
1140 with soft probe scanning electrochemical microscopy. *J. Electroanal. Chem.* **2017**, *786*, 120–128,  
1141 doi:10.1016/j.jelechem.2017.01.015.

- 1142 141. Lesch, A.; Momotenko, D.; Cortés-Salazar, F.; Roelfs, F.; Girault, H. H.; Wittstock, G. High-  
1143 throughput scanning electrochemical microscopy brushing of strongly tilted and curved  
1144 surfaces. *Electrochim. Acta* **2013**, *110*, 30–41, doi:10.1016/j.electacta.2013.03.101.
- 1145 142. Lesch, A.; Chen, P.-C.; Roelfs, F.; Dosche, C.; Momotenko, D.; Cortés-Salazar, F.; Girault, H.  
1146 H.; Wittstock, G. Finger Probe Array for Topography-Tolerant Scanning Electrochemical  
1147 Microscopy of Extended Samples. *Anal. Chem.* **2014**, *86*, 713–720, doi:10.1021/ac403168p.
- 1148 143. Tzu-En, L.; Yu-Jen, L.; Chia-Liang, S.; Horst, P.; Jyh-Ping, C.; Andreas, L.; H., G. H. Soft  
1149 Electrochemical Probes for Mapping the Distribution of Biomarkers and Injected  
1150 Nanomaterials in Animal and Human Tissues. *Angew. Chemie Int. Ed.* **2017**, *56*, 16498–16502,  
1151 doi:10.1002/anie.201709271.
- 1152